the family "O" and the family "U" (Figs. 1 and 2). Two patients in the family "O" and three patients in the family "U" were treated for their seizure disorders and psychiatric symptoms at Kyoto University Hospital. The detailed clinical manifestation of the two families is described in the Results.

Gene analysis

Genetic analysis of ADLTE was approved by the Kyoto University Graduate School of Medicine Ethical Committee, and written informed consent was obtained from all the patients and the control participants investigated in the present study. DNA from the five patients in the four families were analyzed in this study. The control sample consisted of DNA from 50 healthy Japanese volunteers who gave informed consent. Using primers previously reported, eight exons of the *LGI1* gene were amplified and subsequently sequenced on an ABI310 sequencer (Applied Biosystems, Foster City, CA, U.S.A.) (Michelucci et al., 2003). Mutations in the *LGI1* gene were confirmed by NruI restriction enzyme digestion.

RESULTS

Clinical manifestation

Family "O" had a history of epilepsy in nine members in five generations (Fig. 1). A proband, IV-5, a 27-year-old-woman, had the first generalized tonic–clonic seizure (GTCS) at the age of 10 years while asleep. Currently she has GTCSs every 1–2 months, almost daily auras, and weekly complex partial seizure (CPS), despite high-dose polytherapy such as carbamazepine, zonisamide, and clonazepam. The patient had several types of auras as follows. Auditory auras consisted of high-pitched sound,

becoming gradually louder, resulting in inability to understand the spoken language (aphasic state). Visual auras were elementary, flashing light, and metamorphopsia. The patient also had déjà vu, jamais vu, and autonomic auras (i.e., palpitation, cold sweat, and pale face). All of the auras occurred in various combinations and also occurred independently. Those auras, especially the latter ones, were frequently followed by panic attack–like symptoms (i.e., sudden onset of fear and anxiety). The patient also confessed that she had auditory hallucination that she should throw her child out of the window. This occurred independent of the ordinary auras described above. Electroencephalography (EEG) showed no clear epileptiform discharges, despite repetitive sleep EEGs, and magnetic resonance imaging (MRI) showed the small volume of the left superior temporal gyrus. Fluorodeoxyglucose–positron emission tomography (FDG-PET) by statistical parametric mapping (SPM) analysis revealed decreased glucose metabolism in the left lateral temporal area.

The younger sister of the proband, IV-7, a 26-year-old-woman, also had the first GTCS while asleep at the age of 11 years, and currently has GTCSs once a year, and auditory auras (high-pitched sound) and déjà vu, each several times per week. The patient had no visual auras, jamais vu, autonomic auras, or psychiatric symptoms such as anxiety attacks. It was reported that EEG showed no clear epileptiform discharges.

Among their family members, four had apparent psychiatric symptoms such as an outrage of emotion and extraordinary explosive violent behaviors. One of them (II-12) was admitted to the psychiatric hospital for several months, and two of them (II-9 and II-12) had sudden death. Five had both psychiatric symptoms and seizures like the proband. For seizure disorders, at least five (II-12, III-2, III-3, IV-5, and IV-7)
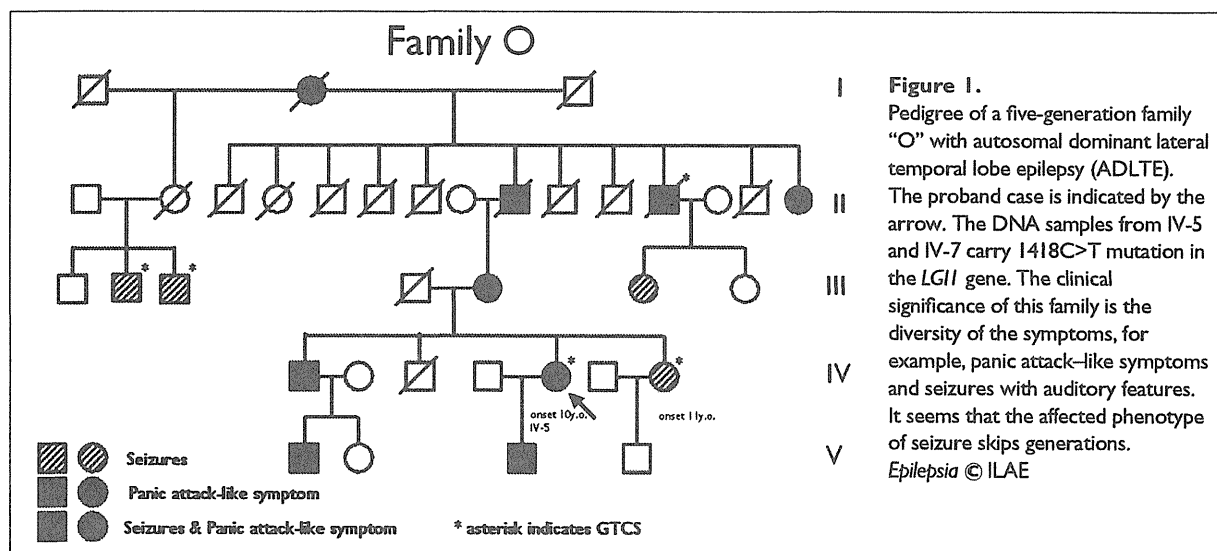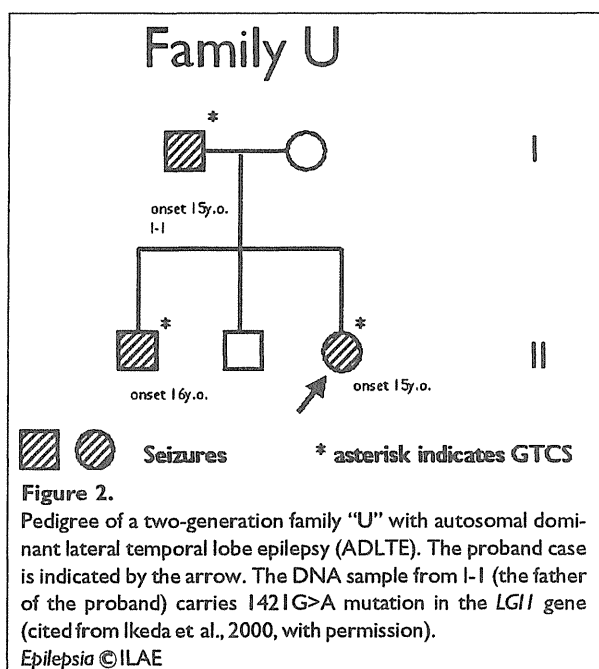

Family O

Figure 1.
Pedigree of a five-generation family "O" with autosomal dominant lateral temporal lobe epilepsy (ADLTE). The proband case is indicated by the arrow. The DNA samples from IV-5 and IV-7 carry 1418C>T mutation in the *LGI1* gene. The clinical significance of this family is the diversity of the symptoms, for example, panic attack–like symptoms and seizures with auditory features. It seems that the affected phenotype of seizure skips generations.
Epilepsia © ILAE

Seizures
Panic attack–like symptom
Seizures & Panic attack–like symptom   * asterisk indicates GTCS

onset 10y.o.
IV-5
onset 11y.o.

Family U

Figure 2.
Pedigree of a two-generation family "U" with autosomal dominant lateral temporal lobe epilepsy (ADLTE). The proband case is indicated by the arrow. The DNA sample from I-I (the father of the proband) carries 1421G>A mutation in the *LGI1* gene (cited from Ikeda et al., 2000, with permission).
Epilepsia © ILAE

		473 474												
Patient S473L	R M	P	L	R	G	S	M	V	F	Q	P	L Q I
Patient R474Q	R M	P	S	Q	G	S	M	V	F	Q	P	L Q I
Human LGI1	R M	P	S	R	G	S	M	V	F	Q	P	L Q I
Dog LGI1	R M	P	S	R	G	S	M	V	F	Q	P	L Q I
Rat LGI1	R M	P	S	R	G	S	M	V	F	Q	P	L Q I
Mouse LGI1	R M	P	S	R	G	S	M	V	F	Q	P	L Q I
Chicken LGI1	R M	P	S	R	G	S	M	V	F	Q	P	L Q I
Fish LGI1	T V	A	S	R	G	S	M	V	F	Q	P	F S V
Human LGI2	A L	P	S	R	G	A	M	T	L	Q	P	F S F
Human LGI3	A L	P	S	R	G	S	L	A	L	Q	P	F L V
Human LGI4	Q L	P	S	R	G	A	H	V	F	Q	P	L L I
Mouse LGI2	A L	P	S	R	G	A	M	T	L	Q	P	F S F
Mouse LGI3	A L	P	S	R	G	S	L	A	L	Q	P	F L V
Mouse LGI4	Q L	P	S	R	G	S	H	V	F	Q	P	L L I

Figure 3.
Multiple amino acid sequence alignment of human LGI1 and other species. The substituted amino acids, serine at the 473rd and arginine at the 474th, are highly conserved throughout other species as well as other subtypes of LGI families.
Epilepsia © ILAE

had both GTCS and partial seizures. Auditory auras were observed in at least two members (III-3 and IV-1).

The phenotype of the family "U" was already reported in detail before the *LGI1* gene was identified as a causative gene of ADLTE in 2002 (Ikeda et al., 2000), and was relatively uniform (Fig. 2). Briefly, I-1, the father of the proband (II-3) was a 51-year-old, full-time employee with a past history of febrile convulsion. At the age of 16 years, his first nocturnal GTCS occurred. His habitual seizures also started with a high-pitched buzzing sound, followed by loss of awareness. The patient often noticed that his seizures were triggered by the telephone bell. His seizures were completely controlled after adding carbamazepine to valproic acid. Two children (II-3 was the proband in Ikeda et al., 2000) also had first GTCS and partial seizures since the second decade, and the seizures were completely controlled by carbamazepine. All of them had normal MRI, and EEG showed sharp transients in the left frontotemporal areas only in I-1, but no clear epileptiform discharges were recorded.

Gene analysis

Sequence analysis of eight exons of *LGI1* in the two patients in family "O" (IV-5 and IV-7 in Fig. 1) revealed point mutation (1418C>T, numbering from the first nucleotide of the initiator codon) resulting in amino-acid substitution of serine to leucine at the 473rd residue. Sequence analysis of DNA from the patient in family "U" (I-1 in Fig. 2) also revealed point mutation (1421G>A) resulting in amino acid substitution of arginine to glutamine at the 474th residue. Each of the two mutations disrupts the

restriction enzyme site of NruI. Digesting polymerase chain reaction (PCR) product of exon 8 with NruI using buffer provided by a manufacturer (New England BioLabos, MA, U.S.A.), the two mutations were screened in control participants. There was neither 1418C>T nor 1421G>A mutation in 50 control participants, suggesting that these base changes could be regarded as mutations, but not polymorphisms.

The serine at residue 473 and arginine at residue 474 of LGI1 were highly conserved between species and its homologs, LGI2, 3, and 4 (Fig. 3). The serine at the 473rd residue was considered to be phosphorylated, and the mutation might disrupt it.

With regard to the clinical features, the reported symptoms in family "O" were consistent with previous reports of ADLTE, except that the degree and incidence of psychiatric symptoms were rather high. Symptoms in family "U" were almost common among pedigrees, except that only II-1 had déjà vu, suggestive of mesial temporal involvement. The two patients in family "O" also had déjà vu; however, other clinical features differed between them.

DISCUSSION

Because all reported ADLTE families with *LGI1* mutations were Caucasians, we presumed that patients with *LGI1*-related epilepsy in Japan were rather rare, or that some genetic backgrounds may lower penetrance rates so that clinically they seem to be sporadic cases even though some families have *LGI1* mutations. In the present study, however, we documented that two independent families in Kyoto province had different *LGI1* mutations.

Clinical manifestations of family "O" were divided into two groups: one had seizures with auditory features and the other with psychiatric symptoms such as explosive

violent behaviors and panic attack–like symptoms. The proband also had apparently nonepileptic auditory hallucination and one member was admitted to the psychiatric hospital. The psychiatric symptoms in ADLTE were also described in the previous reports, but they were much milder. When attention was paid only to seizures with auditory features in this family, epileptic symptoms appeared after skipping two consecutive generations. Therefore, it is most likely that psychiatric symptoms are one of constellations of *LGI1*-related ADLTE. The clinical manifestations of family "O" with *S473L* mutation were different from ones of the British decedent family in Australia, even though they had a mutation identical to our patients (Berkovic et al., 2004).

On the other hand, clinical symptoms of family "U" were nearly uniform, being consistent with previously reported, typical ADLTE. Mutation at the same codon was reported in Spanish family results in premature truncation, and their clinical symptoms were also mild and had the common features of ADLTE (Morante-Redolat et al., 2002).

Recently it was reported that ADAM22 served as a receptor for LGI1, the mutated form of LGI1 failed to bind to ADAM22, and LGI1 enhances α-amino-3-hydroxy-5-methyl-4-isoxazolepropionic acid receptor–mediated synaptic transmission in rat hippocampal slices. (Fukata et al., 2006). Schulte et al. (2006) reported that LGI1 protein assembled into the presynaptic Kv1 channels and inhibited inactivation by Kvbeta1. These findings may suggest that the underlying pathogenetic mechanism of ADLTE would be "loss of function" like other numerous familial epilepsies classified into "channelopathy." However, the diversity of clinical phenotype probably depends on the mutated residue could be explained better by "gain of function" rather than "loss of function" mechanism, which would be resulting in homogenous phenotype. Further genotype–phenotype analyses in patients of different ethnic backgrounds may elucidate a part of the mechanisms.

REFERENCES

Berkovic SF, Izzillo P, McMahon JM, Harkin LA, McIntosh AM, Phillips HA, Briellmann RS, Wallace RH, Mazarib A, Neufeld MY, Korczyn AD, Scheffer IE, Mulley JC. (2004) LGI1 mutations in temporal lobe epilepsies. *Neurology* 62:1115–1119.

Bovo G, Diani E, Bisulli F, Di Bonaventura C, Striano P, Gambardella A, Ferlazzo E, Egeo G, Mecarelli O, Elia M, Bianchi A, Bortoluzzi S, Vettori A, Aguglia U, Binelli S, De Falco A, Coppola G, Gobbi G, Sofia V, Striano S, Tinuper P, Giallonardo AT, Michelucci R, Nobile C. (2008) Analysis of LGI1 promoter sequence, PDYN and GABBR1 polymorphisms in sporadic and familial lateral temporal lobe epilepsy. *Neurosci Lett* 2008 [PMID: 18355961].

Chabrol E, Popescu C, Gourfinkel-An I, Trouillard O, Depienne C, Senechal K, Baulac M, LeGuern E, Baulac S. (2007) Two novel epilepsy-linked mutations leading to a loss of function of LGI1. *Arch Neurol* 64:217–222.

Fertig E, Lincoln A, Martinuzzi A, Mattson RH, Hisama FM. (2003) Novel LGI1 mutation in a family with autosomal dominant partial epilepsy with auditory features. *Neurology* 2003:60.

Fukata Y, Adesnik H, Iwanaga T, Bredt DS, Nicoll RA, Fukata M. (2006) Epilepsy-related ligand/receptor complex LGI1 and ADAM22 regulate synaptic transmission. *Science* 313:1792–1795.

Gu W, Brodtkorb E, Piepoli T, Finocchiaro G, Steinlein OK. (2005) LGI1: a gene involved in epileptogenesis and glioma progression? *Neurogenetics* 6:59–66.

Ikeda A, Kunieda T, Miyamoto S, Fukuyama H, Shibasaki H. (2000) Autosomal dominant temporal lobe epilepsy in a Japanese family. *J Neurol Sci* 176:162–165.

Ikeda A, Kawamata J, Matsumoto R, Takaya S, Usui K, Fukuyama H, Takahashi R. (2007) Variable clinical features in Japanese families with autosomal dominant lateral temporal lobe epilepsy ADLTLE. *Neurol Asia* 12(suppl 1):65.

Kalachikov S, Evgrafov O, Ross B, Winawer M, Barker-Cummings C, Boneschi FM, Choi C, Morozov P, Das K, Teplitskaya E, Yu A, Cayanis E, Penchaszadeh G, Kottmann AH, Pedley TA, Hauser WA, Ottman R, Gilliam TC. (2002) Mutation in LGI1 cause autosomal-dominant partial epilepsy with auditory features. *Nat Genet* 30:335–341.

Michelucci R, Poza JJ, Sofia V, de Feo MR, Binelli S, Bisulli F, Scudellaro E, Simionati B, Zimbello R, D'Orsi G, Passarelli D, Avoni P, Avanzini G, Tinuper P, Biondi R, Valle G, Mautner VF, Stephani U, Tassinari CA, Moschonas NK, Siebert R, Lopez de Munain A, Perez-Tur J, Nobile C. (2003) Autosomal dominant lateral temporal epilepsy: clinical spectrum, new epitempin mutations, and genetic heterogeneity in seven European families. *Epilepsia* 44:1289–1297.

Morante-Redolat JM, Gorostidi-Pagola A, Piquer-Sirerol S, Sáenz A, Poza JJ, Galán J, Gesk S, Sarafidou T, Mautner VF, Binelli S, Staub E, Hinzmann B, French L, Prud'homme JF, Passarelli D, Scannapieco P, Tassinari CA, Avanzini G, Martí-Massó JF, Kluwe L, Deloukas P, Moschonas NK, Michelucci R, Siebert R, Nobile C, Pérez-Tur J, López de Munain A. (2002) Mutations in the LGI1/Epitempin gene on 10q24 cause autosomal dominant lateral temporal epilepsy. *Hum Molec Genet* 11:1119–1128.

Ottman R, Risch N, Hauser WA, Pedley TA, Lee JH, Barker-Cummings C, Lustenberger A, Nagle KJ, Lee KS, Scheuer ML, Neystat M, Susser M, Wilhelmsen KC. (1995) Localization of a gene for partial epilepsy to chromosome 10q. *Nat Genet* 10:56–60.

Schulte U, Thumfart JO, Klöcker N, Sailer CA, Bildl W, Biniossek M, Dehn D, Deller T, Eble S, Abbass K, Wangler T, Knaus HG, Fakler B. (2006) The epilepsy-linked Lgi1 protein assembles into presynaptic Kv1 channels and inhibits inactivation by Kvbeta1. *Neuron* 49:697–706.

Loss of PINK1 in medaka fish (Oryzias latipes) causes late-onset decrease in spontaneous movement

Hideaki Matsui [a,b], Yoshihito Taniguchi [b,c], Haruhisa Inoue [a,b], Yoshito Kobayashi [a], Yoshiyuki Sakaki [d,1], Atsushi Toyoda [d,2], Kengo Uemura [a,b], Daisuke Kobayashi [e], Shunichi Takeda [b,c,*], Ryosuke Takahashi [a,b,**]

[a] Department of Neurology, Kyoto University, Graduate School of Medicine, 54 Shogoin-Kawahara-cho, Sakyo-ku, Kyoto 606-8507, Japan
[b] Core Research for Evolutional Science and Technology (CREST), Japan Science and Technology Agency, Japan
[c] Department of Radiation Genetics, Kyoto University, Graduate School of Medicine, Yoshida-Konoe-cho, Sakyo-ku, Kyoto 606-8501, Japan
[d] RIKEN Genomic Sciences Center, Yokohama 230-0045, Japan
[e] Department of Anatomy and Developmental Biology, Kyoto Prefectural University of Medicine, Kyoto 602-0841, Japan

ABSTRACT

Parkinson's disease is a neurodegenerative disease associated with the degeneration of dopaminergic neurons in the substantia nigra. The PTEN-induced kinase 1 gene (PINK1) is responsible for recessive inherited familial Parkinson's disease (PARK6). Neither the function of PINK1 nor its role in the prevention of Parkinson's disease is fully understood. Gene disruption of PINK1 causes remarkably different phenotypes in animal models such as Drosophila melanogaster, zebrafish, and mouse, none of which recapitulate Parkinson's-disease-like symptoms. We established PINK1-gene-disrupted medaka fish. These mutant fish grew normally at first, then developed significant decrease in the frequency of spontaneous swimming movements in the late-adult stage. Although the mutants did not show any dopaminergic cell loss, the amount of 3,4-dihydroxyphenylacetic acid, a major metabolite of dopamine, decreased. Thus, PINK1 contributes to the maintenance of dopamine metabolism, even before the selective death of dopaminergic neurons. Our animal model is therefore a valuable tool to detect pathogenesis in Parkinson's patients in the early stages.

© 2009 Elsevier Ireland Ltd and the Japan Neuroscience Society. All rights reserved.

1. Introduction

Parkinson's disease (PD) is the second-most common neurodegenerative disease among humans. It is associated with the degeneration of dopaminergic neurons in a subset of neuronal populations represented by the substantia nigra pars compacta in the midbrain. Although the majority of cases develop sporadically, 5–10% of PD patients are familial, with the disease caused by gene mutation (Gasser, 2005). To date, 10 different genes responsible for familial PD have been identified. The functional analysis of these genes is important to our understanding of the molecular

pathogenesis of PD. Recessive inherited familial PD (PARK6) is attributable to mutations in the PINK1 gene (Valente et al., 2004). These mutations appear to compromise the function of the PINK1 protein (Sim et al., 2006).

PINK1 is a highly conserved 581 amino acid protein. The gene is ubiquitously expressed in the human brain (Gandhi et al., 2006) and seems to be activated by a tumor suppressor, PTEN (Unoki and Nakamura, 2001). The PINK1 gene encodes a kinase and contains a mitochondria-targeting motif. One of the putative substrates of the kinase is TNF receptor-associated protein 1 (TRAP1), though its biological significance remains elusive (Pridgeon et al., 2007). PINK1 plays a protective role against oxidative stress and MPTP (Wood-Kaczmar et al., 2008; Haque et al., 2008). Silencing of the PINK1 gene results in mitochondrial pathology in the human cell line (Exner et al., 2007).

Gene disruption of PINK1 causes distinctly different phenotypes in different animal models. Mice deficient in PINK1 exhibit impaired dopamine release, but not movement disorders or dopaminergic cell death (Kitada et al., 2007). Loss of PINK1 function in Drosophila melanogaster results in a drastic phenotype that includes male sterility and the degeneration of both muscle and dopaminergic neurons with massive mitochondria-related pathology (Clark et al., 2006; Park et al., 2006; Yang et al., 2006). In

zebrafish, depletion of PINK1 during development causes severe developmental disorders and neurodegeneration (Anichtchik et al., 2008). None of these animal models for PARK6 faithfully recapitulate the pathology of human PD.

In this study, we generated *PINK1* mutant medaka fish by screening our TILLING library (Taniguchi et al., 2006). The *PINK1* mutant medaka showed normal phenotypes for germ-cell lineage, skeletal muscle, and mitochondrial morphology. However, they showed a significant decrease in spontaneous movement during the late stages of life as well as deregulation of dopamine metabolism. The *PINK1* mutant medaka therefore provides a unique opportunity to analyze the causal relationship between dopamine metabolism and neurological symptoms.

2. Materials and methods

2.1. Cloning of medaka PINK1 gene

RNA was extracted from *wild-type* medaka embryos by Trizol (Invitrogen) according to the manufacturer's instructions. cDNA was synthesized using SuperScript III (Invitrogen). To identify medaka *PINK1* orthologs, we used the basic local alignment search tool (BLAST) to search the medaka genome database (http://dolphin.lab.nig.ac.jp/medaka/). Medaka *PINK1* cDNA sequences were then determined using a combination of RT-PCR and rapid amplification of cDNA ends (RACE). RACE products were generated using Seegene's Capfishing kit (Seegene). The 5′ RACE (CCATAGGC-CAAGGGCTTGAGCGGGC) and 3′ RACE primers (CCAGTGCCCCC-GCTGATGTGCAGTTAGT) were used. The cDNA sequence was used to retrieve the genomic sequence from the draft medaka genome assembly.

2.2. Generation of PINK1 mutant medaka

Generation of *PINK1* mutant medaka was carried out as described previously (Taniguchi et al., 2006). To find the mutations in the region of interest, the genome sequence was amplified with forward primer #1 (TCGGCTTCTACAAGGCTGTT) and reverse primer #1 (CACCCAACTGTGGCTAGTGA) by PCR (92 °C for 60 s; 12 cycles of 92 °C for 20 s, 65 °C for 20 s with a decrement of 0.6 °C per cycle, 72 °C for 30 s; 20 cycles of 92 °C for 20 s, 58 °C for 20 s and 72 °C for 30 s; 72 °C for 180 s [T1 Thermocycler, Biometra]). Sequences were analyzed for the presence of heterozygous mutations using the reverse primer #1. *In vitro* fertilization was carried out using sperm with the desired mutation and the progeny were genotyped by sequencing. Heterozygous fish carrying the same mutation were back-crossed with *Kyoto-Cab*, a substrain of *Cab*, at least 4 times. Furthermore, all the experiments were reproduced using fish back-crossed 7 times or more. Heterozygous fish with this mutation were incrossed to obtain homozygous fish. To verify the genotype of the progeny from this incross, the genome was amplified with forward primer #2 (CAGATTGG-GAAAGGATCCAA) and reverse primer #2 (CCCAAAGTTCCACAG-CATCT). PCR was carried out according to the following thermocycling program: 94 °C for 120 s; 35 cycles of 94 °C for 30 s, 62 °C for 30 s, 72 °C for 30 s; and 72 °C for 120 s (GeneAmp PCR system9700, Applied Biosystems). 1 μl of PCR product was used as a template for sequencing using BigDYE (Applied Biosystems). Sequencing products were purified by magnetic beads and analyzed using the ABI 3700 DNA Sequencer (Applied Biosystems), following the standard protocol.

2.3. Semi-quantitative RT-PCR

RNA was extracted from the brain for each genotype with Trizol (Invitrogen). cDNA was synthesized using 1 μg RNA for each genotype with SuperScript III (Invitrogen). mRNA expression levels were determined by PCR. For *PINK1*, PCR was carried out using the following thermocycling program: 94 °C for 120 s; 28 cycles at 94 °C for 30 s, 68 °C for 30 s, 72 °C for 30 s; and 72 °C for 120 s (T1 Thermocycler, Biometra). For *β-actin*, the thermocycling program was 94 °C for 120 s; 20 cycles at 94 °C for 30 s, 61 °C for 30 s, 72 °C for 30 s; and 72 °C for 120 s (T1 Thermocycler, Biometra). Forward primer #3 (GAACAGAGCCGTCTTTCTGG) and reverse primer #3 (CCCAAAGTTCCACAGCATCT) were used for *PINK1*. The forward primer (ACTACCTCATGAAGATCCTG) and the reverse primer (TTGCTGATCCACATCTGCTG) were used for *β-actin*.

2.4. In situ hybridization

The digoxigenin (DIG) labeled riboprobe was generated with the DIG RNA labeling kit according to the manufacturer's instructions (Roche). Medaka brains were fixed in freshly prepared 4% paraformaldehyde in PBST. Brains were dehydrated sequentially in methanol. After rehydration, the specimens were treated with 10 μg/ml proteinase K, and treated again in the same fixative for 25 min. The specimens were pre-hybridized in hybridization buffer (HB, 50% formamide, 5× SSC, 5 mg/ml yeast tRNA, 100 μg/ml heparin, 0.1% Tween-20) at 65 °C for 2 h, and then brains were hybridized overnight with the riboprobe in hybridization buffer at 65 °C. Subsequently, brains were washed in decreasing concentrations of SSCT. For probe detection, the embryos were incubated in 0.2% blocking solution (Roche) for 2 h and then rocked overnight with anti-DIG antibody conjugated with alkaline phosphatase (1:7000 dilution, Roche) in 0.2% blocking solution at 4 °C. After several washes with PBST, hybridized probe was detected via color reaction with 450 μg/ml NBT and 175 μg/ml BCIP (Roche). The color reaction was stopped by PBST. Samples were fixed in 4% paraformaldehyde in PBST for 20 min, then embedded in paraffin. Specimens were sliced into 7 μm sections.

2.5. High performance liquid chromatography

Medaka brains were homogenized in 100 μl of 0.4 M $HClO_4$ containing 4 mM $Na_2S_2O_5$ and 4 mM diethylenetriaminepentaacetic acid. Supernatant by centrifugation at 18,500 × g for 5 min was used to measure free catechols. High performance liquid chromatography (HPLC) was conducted with a mobile phase containing buffer A:acetonitrile:methanol (1000:25.9:62.9, v/v) (buffer A: 0.1 M phosphate, 0.05 M citrate, 4 mM sodium 1-heptanesulfonate and 0.1 mM EDTA, pH 3.0). Catecholamine and its metabolites were identified using a series coulometric detector (ESA, Inc.). Data were collected and processed using CHROME-LEON™ Chromatography Data Systems 6.40 (Dionex). The pellet was reserved for analysis of the protein content. For this purpose, the pellet was solubilized in 100 μl of 0.5N NaOH at 60 °C and the protein was quantified by means of a BCA assay (Pierce) using bovine serum albumin (BSA) as the standard.

2.6. Hematoxylin–eosin staining

Entire medaka bodies or individual organs were fixed in 4% paraformaldehyde for 24 h, embedded in paraffin, then sliced into 10-μm sections. Hematoxylin–eosin (HE) staining was done using standard protocols.

2.7. Transmission electron microscope and Toluidine blue staining

To prepare for electron microscopy, male testes and muscle tissue were fixed overnight in 2% gluteraldehyde with a 0.1 M cacodylate buffer. After rinsing in a 0.1 M cacodylate buffer with 0.1 M sucrose, samples were postfixed in 1% OsO_4, with a 0.1 M

cacodylate buffer and 0.1 M sucrose for 1.5 h. Samples were rinsed, dehydrated in an ethanol series, and embedded in Epon. The 1-μm sections were stained with Toluidine blue, and the 50–80 nm sections were stained with uranyl acetate and lead citrate.

2.8. Immunohistochemistry

Medaka brains were fixed in 4% paraformaldehyde for 24 h and embedded in paraffin. Each brain was sliced into 20 μm sections to prepare for TH immunohistochemistry. Immunohistochemical analysis (1:500, mouse anti-TH, MAB318, Millipore) was carried out on every section using the Vector Elite ABC kit with DAB. The number of dopaminergic neurons in the middle diencephalon was determined by counting the TH-immunopositive (TH$^+$) neurons in the coronal sections using an OLYMPUS BX51 microscope with a MICROFIRE digital camera (Olympus) and Stereo Investigator (MBF Bioscience).

2.9. TdT-mediated dUTP nick-end labeling assay

Brains were fixed in 4% paraformaldehyde for 24 h and embedded in paraffin. Each brain was sliced into 5 μm sections in preparation for a TUNEL assay. Apoptotic cells were detected by the TUNEL method using an in situ Apoptosis Detection Kit (TaKaRa Bio Inc.), according to the manufacturer's protocol.

2.10. Western blot analysis

Brains were homogenated in a RIPA buffer (25 mM Tris–HCl [pH 7.6], 150 mM NaCl, 1% NP-40, 1% sodium deoxycholate, 0.1% SDS) with protease inhibitors and processed for SDS-PAGE analysis. Immunoreactive bands were detected with ECL reagent or ECL plus reagent (GE Healthcare Life Sciences) and the chemiluminescent signal was visualized by exposing the membrane to Fuji RX X-ray film (Fuji Film). The film was scanned and densitometric analysis of blots was performed using ImageJ software (National Institute of Health). The background intensity of the film was subtracted from the band intensity. Anti-medaka parkin polyclonal antibody was raised against full-length medaka parkin protein and used for the analysis (1:500). Anti-TH monoclonal antibody (1:1000, mouse anti-TH, MAB318, Millipore) was used for the Western blot analysis of the TH. Anti-β-actin monoclonal antibody (1:5000, AC-15, Sigma–Aldrich) was used for the loading control. Parkin-deficient medaka, used for a negative control, was generated as described previously (Taniguchi et al., 2006).

2.11. Behavioral analysis

The medaka were tested for spontaneous swimming. Images were collected using a video camera positioned above the tank under low intensity, indirect white light, then analyzed by a computer-assisted system (Muromachi Kikai). The water tank was a transparent circular container (20 cm diameter, 2 cm water depth, 27 °C). Upon introduction into the tank, all adult fish remained motionless for several minutes, then began to swim. Filming began 1 min after the medaka began to swim and lasted for 5 min. We defined movement as occurring when a medaka moved more than 0.1 cm per 0.1 s. Total swimming distance (cm), duration of swimming movement (s) and swimming velocity (total swimming distance/duration of swimming movement) were measured and compared across groups.

2.12. Statistical analysis

Data were expressed as mean ± standard error of the mean (SEM). Results were statistically evaluated for significance using the ANOVA test with post hoc analysis using Dunnet's test or logrank test for survival analysis. Differences were considered significant when $p < 0.05$.

3. Results

3.1. Cloning of medaka PINK1

Only a single ortholog of the human PINK1 gene was identified (by BLAST search) in the draft medaka genome. The medaka PINK1 gene has 8 exons and encodes a protein consisting of 577 amino acids (Fig. 1A and B). The medaka PINK1 amino acid sequence has 54.1% homology to human PINK1. The kinase domain was highly conserved between the two species (Fig. 1B).

3.2. Generation of PINK1 mutant medaka

To generate PINK1 mutant medaka, we targeted exons 2 and 3 of the PINK1 gene for nucleotide sequencing. We sequenced the genomes of 5771 samples obtained from ENU-mutagenized medaka. We identified 14 mutations in total, 6 of which were silent mutations (Table 1). From the eight other mutations, we selected a nonsense mutation, Q178X, for further study because it resulted in the disruption of the kinase domain. It has been reported that human PARK6 patients carry similar truncation mutations (Q239X, R246X, Y258X, W437X, Q456X, R492X) in the kinase domain (Valente et al., 2004; Hedrich et al., 2006; Hatano et al., 2004; Tan et al., 2006).

From the incross of heterozygous Q178X mutant parents, we obtained the expected numbers (according to Mendelian inheritance [Fig. 3A]) of wild-type fish ($PINK1^{WT/WT}$), heterozygous mutants ($PINK1^{WT/Q178X}$), and homozygous mutants ($PINK1^{Q178X/Q178X}$) (Fig. 2A). Semi-quantitative RT-PCR showed a marked reduction of PINK1 mRNA in the $PINK1^{Q178X/Q178X}$ medaka, probably due to the nonsense-mediated mRNA decay (Fig. 2B). We therefore concluded that we had succeeded in generating PINK1-deficient medaka fish.

3.3. Distribution of medaka PINK1 mRNA

To characterize medaka PINK1 expression, we visualized medaka PINK1 mRNA by in situ hybridization. The anti-sense RNA probe exhibited diffuse signals in the gray matter of $PINK1^{WT/WT}$ medaka brain (Fig. 4A–E). The telencephalon and diencephalon that contain striatum and many dopaminergic neurons respectively showed moderate anti-sense signals (Fig. 4A–C). The optic tectum disclosed relatively intense signals comparing to other regions (Fig. 4B and C). On the other hand, the signals of hindbrain and spinal cord were weak (Fig. 4D and E). We further investigated medaka PINK1 mRNA expression in $PINK1^{Q178X/Q178X}$ medaka. In this case, we could not detect the signals of anti-sense probe (Fig. 4F–J). This finding suggested the signals of anti-sense probe was specific to medaka PINK1 mRNA and again supported the degradation of PINK1 mRNA in $PINK1^{Q178X/Q178X}$ medaka.

3.4. $PINK1^{Q178X/Q178X}$ medaka showed normal development and mild shortening of life span

Like human PARK6 patients, $PINK1^{Q178X/Q178X}$ medaka grew normally for 12 months without any obvious morphological abnormalities or developmental disorders. Remarkably, the $PINK1^{Q178X/Q178X}$ medaka showed a significant decrease in life span, when compared with $PINK1^{WT/WT}$ and $PINK1^{WT/Q178X}$ fish (the $PINK1^{Q178X/Q178X}$ medaka began to die at 12 months) (Fig. 3B). This diminished life expectancy was not caused by increased tumorigenesis (data not shown).
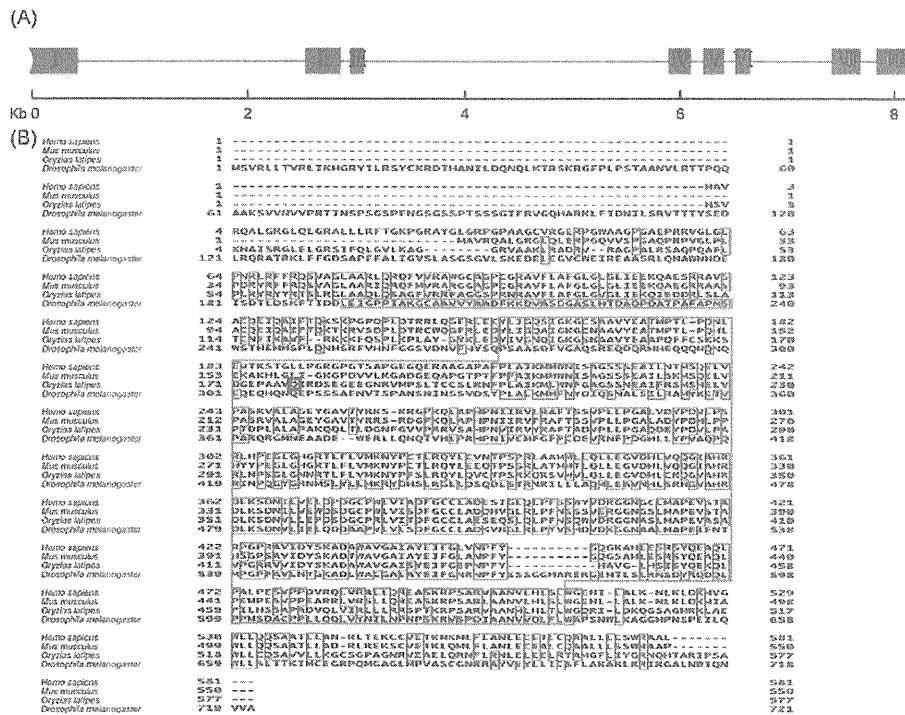
(A)

(B)

Fig. 1. Medaka PINK1 profiles. (A) Genome structure of medaka *PINK1* gene. The red boxes indicate each exon (with the Greek numeral representing the number of the exon) and the bar represents the intron. (B) Sequence alignment of human, mouse, medaka and *Drosophila melanogaster* PINK1 protein. Amino acids conserved among three or four species are outlined in red. The medaka PINK1 amino acid sequence has 54.1% homology to human PINK1. The kinase domain, which is highly conserved across the two species, is outlined in light blue. The green outlining signifies the Q178X mutation in the mutant medaka. (For interpretation of the references to color in this figure legend, the reader is referred to the web version of the article.)

3.5. PINK1$^{Q178X/Q178X}$ medaka show reduced body weight at the late-adult stage

To investigate the cause of this shortened life expectancy, we measured the body weight of the PINK1$^{Q178X/Q178X}$ medaka over time. We placed ten 8-month-old fish from each genotype into separate tanks for 4 months. There was no significant difference in body weight among medaka with the PINK1$^{WT/WT}$, PINK1$^{WT/Q178X}$, and PINK1$^{Q178X/Q178X}$ genotypes during this time (Fig. 5A). Nor were there significant differences in body weight when medaka representing all three genotypes were maintained together in one

Table 1
List of *PINK1* mutations from our TILLING library showing mutated nucleotides and resulting changes of the transcript.

DNA sequence	Amino acid substitution	Result
AGGACACTTC (A>G) TTTACATACC		Intron
TGCAGGCGGT (G>A) TTCAGAAAGA	V121V	Silent
AAAGAAGAAG (T>C) TCCAGAGCCC	F127L	Substitution
AACTGGAGGA (T>C) TACATTGTAG	D142D	Silent
AAAGGATCCA (A>G) CGCAGCTGTG	N154S	Substitution
GCTGTGTATG (A>G) AGCTGCACCT	E159G	Substitution
CCAAGAAAAG (C>T) GATGGTGAGC	S170S	Silent
CGCCGCGGTG (C>T) AGATACGAGA	Q178X	Truncation
GCTGTGGAAC (T>C) TTGGGGTGGG	F212L	Substitution
TGTGATTCTA (T>A) GTGTTTGCAG		Intron
TTCCCACAGA (C>T) CCCCTCGCTC	D233D	Silent
CGCTCTGGCC (C>A) CAGCAAAACA	P239T	Substitution
GCTCTGGCGC (C>T) AGCAAAACAG	P239L	Substitution
CGCCAGCAAA (A>G) CAGCAACTTA	K241K	Silent

(A>B): A is the nucleotide of *wild-type* Kyoto-cab and B is the nucleotide of the mutant. Of the 14 types of mutation in the genome, 2 were located in the intron, 5 resulted in silent change of the amino acid sequence, 6 were amino acid substitutions and 1 was a truncation of the transcript. The mutation we selected (Q178X) is underlined.

tank for 8 months. However, at 12 and 18 months, the body weight of the PINK1$^{Q178X/Q178X}$ medaka increased at a slower rate, compared with the PINK1$^{WT/Q178X}$ and PINK1$^{Q178X/Q178X}$ medaka when all the genotypes were maintained together (Fig. 5B). These findings imply that older PINK1$^{Q178X/Q178X}$ medaka were not able to compete for limited amounts of food with littermates carrying the other genotypes.

3.6. Muscle, sperm, and mitochondria intact in PINK1$^{Q178X/Q178X}$ medaka

PINK1-deficient *Drosophila* show male sterility, skeletal muscle and sperm degeneration, and abnormal mitochondria morphology. We therefore inspected the morphology of these tissues in medaka. Contrary to the *Drosophila* model, the skeletal muscle and sperm appeared to be normal in the PINK1$^{Q178X/Q178X}$ medaka (Fig. 6A–D). Nor did the mitochondria in the skeletal muscle (Fig. 6E and F) or sperm show any abnormal morphology (data not shown). Both male and female PINK1$^{Q178X/Q178X}$ medaka were consistently fertile (data not shown). Thus, deletion of PINK1 causes a significantly less abnormal phenotype of muscle and sperm in medaka than in *Drosophila*.

3.7. Amount of parkin indistinguishable across genotypes

Familial PD (PARK2) is caused by mutations of the gene-encoding E3 ubiquitin ligase, *parkin* (Kitada et al., 1998). Since studies of the *PINK1*-silenced zebrafish and *D. melanogaster* found a reduction of *parkin* mRNA and parkin protein, respectively (Anichtchik et al., 2008; Yang et al., 2006), we used Western blot analysis to measure parkin protein. The amount of parkin was comparable in the PINK1$^{WT/WT}$, PINK1$^{WT/Q178X}$, and PINK1$^{Q178X/Q178X}$ medaka (Fig. 7).
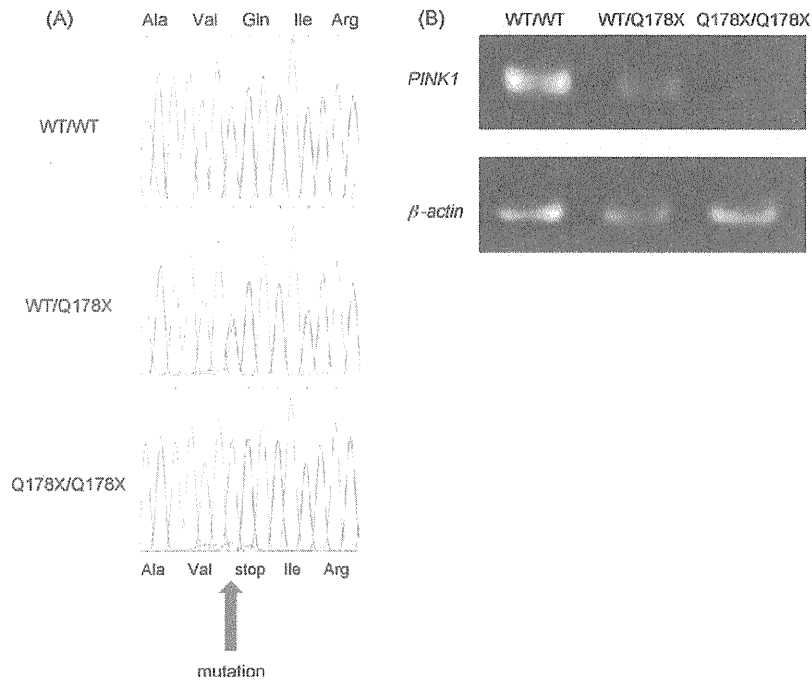
Fig. 2. Generation of $PINK1^{Q178X/Q178X}$ medakas. (A) Sequence data for each genotype. A = green, T = red, G = black, and C = blue. The three-letter amino acid codes show the resulting transcript. The top figure illustrates the $PINK1^{WT/WT}$ medaka sequence, while the middle and bottom figures illustrate heterozygous and homozygous Q178X mutation in $PINK1^{WT/Q178X}$ and $PINK1^{Q178X/Q178X}$ medaka, respectively. The C to T mutation of the genome results in a TAG stop codon (red arrow). (B) Semi-quantitative RT-PCR of $PINK1$ mRNA for each genotype. The upper and lower lanes show the RT-PCR results of $PINK1$ and β-actin (control) mRNA, respectively. The $PINK1$ mRNA of the $PINK1^{Q178X/Q178X}$ medaka decreased markedly compared with $PINK1^{WT/WT}$ and $PINK1^{WT/Q178X}$. This reduction may be due to nonsense-mediated mRNA decay. (For interpretation of the references to color in this figure legend, the reader is referred to the web version of the article.)

3.8. No significant dopaminergic cell loss in $PINK1^{Q178X/Q178X}$ medaka

Dopaminergic cell loss and the denervation of the striatum constitute the representative pathology of human PD patients. Having previously identified tyrosine-hydroxylase-positive (TH⁺) dopaminergic neurons and noradrenergic neurons in the medaka
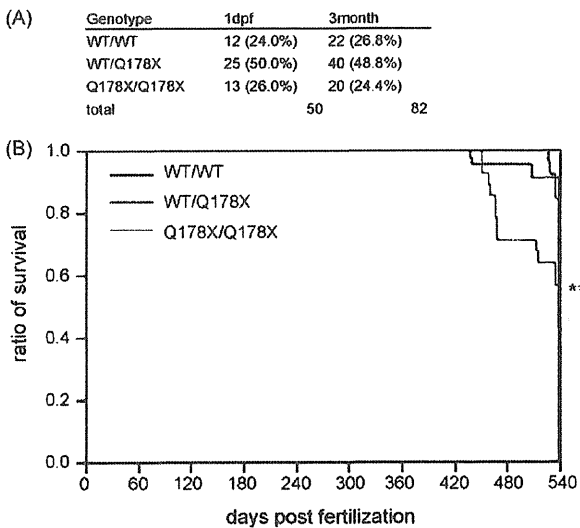

Fig. 3. Mendelian inheritance of Q178X mutation and survival curves of $PINK1^{Q178X/Q178X}$ medaka. (A) The ratio of genotypes in newborn and 3-month-old medaka with $PINK1^{WT/Q178X}$ parents. Both results agree with Mendelian inheritance. These Mendelian ratios suggest no difference in mortality rates in the developmental/larval stage. (B) Survival curve for each genotype. End point is the death of each medaka or day 540. The results show mild but significant shortening of the life span in $PINK1^{Q178X/Q178X}$ medaka ($n = 28$), comparing with $PINK1^{WT/WT}$ ($n = 26$) or $PINK1^{WT/Q178X}$ ($n = 46$). ***$p < 0.001$ vs. $PINK1^{WT/WT}$.

brain, as well as selective loss of TH⁺ dopaminergic neurons in MPTP-treated medaka (Matsui et al., 2009), we histologically examined the TH⁺ neurons. The number of cells in the middle diencephalon did not decrease in the $PINK1^{Q178X/Q178X}$ medaka, when compared with medaka carrying the other genotypes, even at 18 months (Fig. 8A–E). Western blot analysis of the whole brain indicated a similar amount of TH protein in each genotype (Fig. 8I). The $PINK1^{Q178X/Q178X}$ medaka did not display pathological abnormalities in dopaminergic neurons in other regions or in noradrenergic neurons in the medulla oblongata (data not shown). We continued to inspect TH immunohistochemistry, focusing on the striatum, because we previously found that the striatum contains the terminals of dopaminergic neurons, and also because denervation of the striatum is observed in human PD patients. The distribution of dopaminergic neurons in the striatum showed no detectable abnormalities in the $PINK1^{Q178X/Q178X}$ medaka (Fig. 8G and H). To analyze apoptotic cells, we performed a TUNEL assay on the whole brain. Virtually no apoptotic cell death was present in either the $PINK1^{Q178X/Q178X}$ or the control medaka (data not shown). In sum, the $PINK1^{Q178X/Q178X}$ medaka showed no prominent defect in the number or morphology of dopaminergic and noradrenergic neurons.

3.9. Abnormal amount of dopamine and DOPAC in the absence of PINK1 in the brains of young and old fish

A decreased amount of catecholamine is the most prominent feature of human PD patients. We therefore measured the amount of dopamine and norepinephrine in the whole brain of $PINK1^{Q178X/Q178X}$ medaka at 4, 8, 12 and 18 months. The amount of norepinephrine did not differ across genotypes (Fig. 9C). Unlike with human PD patients, the amount of dopamine in the medaka carrying $PINK1^{Q178X/Q178X}$ as well as the other genotypes was very similar at 12 and 18 months. However, to our surprise, the amount
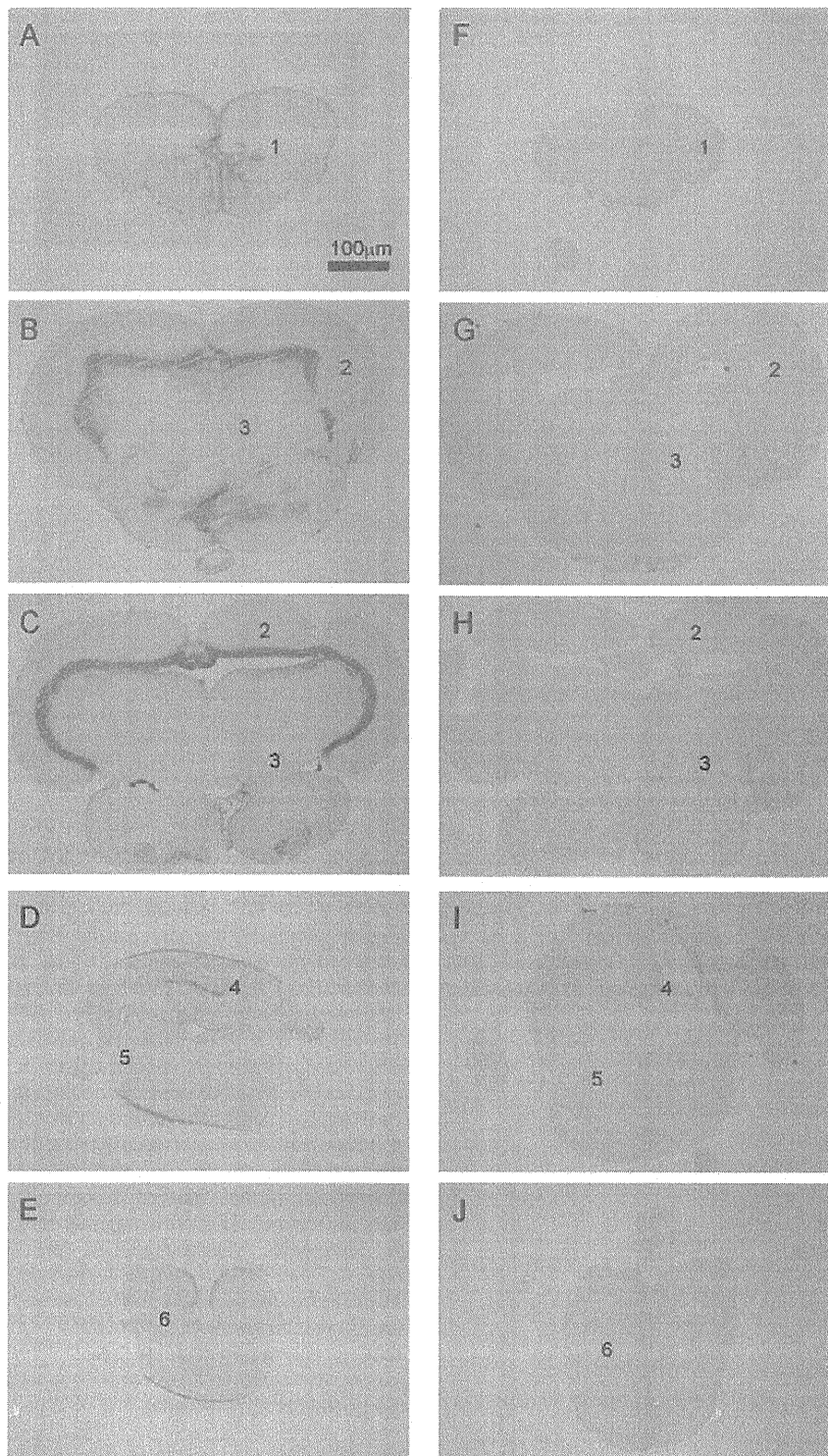
Fig. 4. In situ hybridization of medaka PINK1 mRNA. Anti-sense signals of $PINK1^{WT/WT}$ medaka brain (A–E) and $PINK1^{Q178X/Q178X}$ medaka brain (F–J) (12 months). (1) Telencephalon, (2) optic tectum, (3) diencephalon, (4) cerebellum, (5) medulla oblongata and (6) spinal cord.

of dopamine in the $PINK1^{Q178X/Q178X}$ medaka brain was higher than that of the $PINK1^{WT/WT}$ at both 4 and 8 months (Fig. 9A). By 12 months, the levels of dopamine were the same for all genotypes, and they remained the same at 18 months (Fig. 9A). If the elevated dopamine were functional, these fish might be expected to move more frequently than fish carrying the other genotypes. In fact, the

$PINK1^{Q178X/Q178X}$ medaka moved less frequently than did the fish carrying the other genotypes (Fig. 10A–C), suggesting that the elevated dopamine levels reflect deregulation of dopamine metabolism, including the defective release of dopamine from the neurons. This idea is supported by the fact that the amount of 3,4-dihydroxyphenylacetic acid (DOPAC), a metabolite of dopa-
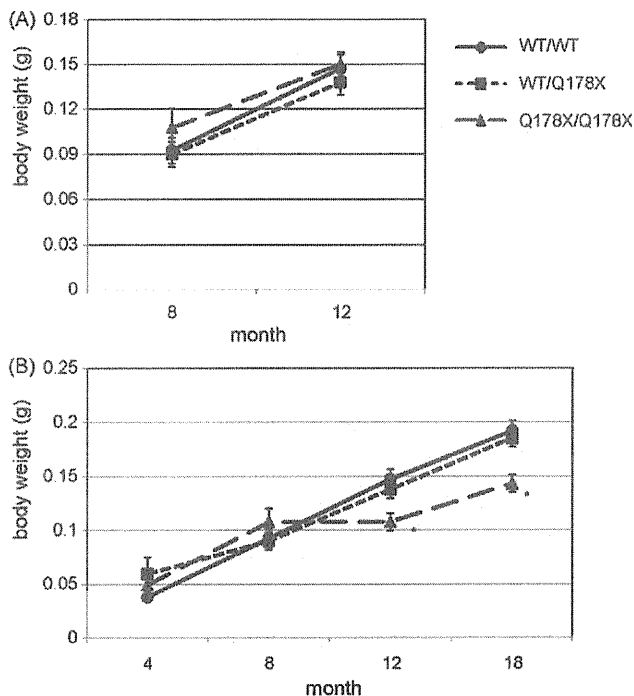
Fig. 5. Body weight of $PINK1^{Q178X/Q178X}$ medaka. (A) Body-weight curves for fish separated by genotype at 8 months. No significant differences were seen ($n = 10$ for each group). (B) Body-weight curves for fish not separated by genotype. A reduced increase in body weight was observed for the $PINK1^{Q178X/Q178X}$ medaka at 12 and 18 months ($n = 15$ for each group). *$p < 0.05$ vs. $PINK1^{WT/WT}$.

mine, decreased. We conclude that the loss of PINK1 causes dysregulation of dopamine metabolism without affecting the survival of dopaminergic neurons.

3.10. $PINK1^{Q178X/Q178X}$ mutation causes reduction of spontaneous swimming only at 12 and 18 months

Late-onset reduction of spontaneous movement is one of the key symptoms found in human PD patients. We therefore quantified spontaneous swimming movement in $PINK1^{Q178X/Q178X}$ medaka. All fish showed comparable movement at 4 and 8 months, irrespective of the genotype of the $PINK1$ gene. Remarkably, the $PINK1^{Q178X/Q178X}$ medaka displayed a significant reduction of spontaneous swimming at 12 and 18 months, in comparison with fish carrying the other genotypes (Fig. 10A–D). These significant decreases were confirmed by all examined swimming parameters: total distance, duration of movement, and velocity. We therefore conclude that the loss of PINK1 causes late-onset reduction of spontaneous swimming movement.

4. Discussion

Japanese medaka (*Oryzias latipes*) is easy to handle and produce large numbers of progeny per generation. It has several advantages over zebrafish in modeling PD. First, the whole genome has been sequenced and assembled since the size of medaka genome is only 700 Mb, half the size of the zebrafish genome. Second, several inbred strains have been established in medaka, but not in zebrafish. The lack of genetic variations among individuals may simplify and facilitate genetic studies, and is particularly important for disease models. Third, cryopreservation of the sperm is easy and reliable, so we can maintain and store numerous strains in the laboratory. Considering the merits that are above-

mentioned, we can regard medaka as one of the attractive vertebrate (*Drosophila* is not vertebrate) animal models.

In this report, we verified that the $PINK1^{Q178X/Q178X}$ medaka is a novel animal model suitable for use to investigate the pathogenesis of PD. Mutant fish display a phenotype very close to that of human PD patients. This phenotype includes normal development and growth, mild shortening of the life span, late-onset reduction of spontaneous movement, and a decrease in the amount of dopamine metabolic product (DOPAC). The establishment of the medaka PD model will allow for extensive genetic analysis in the future, using multiple gene disruption and expression of transgenes with large numbers of fish.

By analyzing the medaka PD model over time, we were able to determine the level of dopamine and its metabolic products in the brain. We found that the loss of PINK1 function affects the metabolism of dopamine in the central nervous system. Indeed, the amount of DOPAC decreased between the 4 and 18 months. Unexpectedly, we observed a higher, rather than a lower, amount of dopamine in the brains of 4- and 8-month-old $PINK1^{Q178X/Q178X}$ medaka compared to $PINK1^{WT/WT}$. This appears to be similar to the results of a study using $PINK1$-shRNA-expressing transgenic mice, which showed increased amounts of dopamine (Zhou et al., 2007). In another study, gene disruption of $PINK1$ was found to impair the release of dopamine from neurons in the striatum, though the dopamine levels were not documented (Kitada et al., 2007). In our study, the increased level of dopamine was not associated with an increase in spontaneous movement in young $PINK1^{Q178X/Q178X}$ medaka. Taking these observations together, it seems that one possible scenario is that the $PINK1^{Q178X/Q178X}$ medaka are incapable of effectively releasing dopamine as a neuronal transmitter, leading to the accumulation of dopamine in the neuronal cells. This accumulated dopamine might harm the neurons, because the metabolism of dopamine is accompanied by the generation of oxidative radical species (Blum et al., 2001). Whether or not the amount of dopamine also increases in the brain of human PARK6 patients prior to the appearance of PD-related symptoms should be investigated.

The late-adult-onset phenotype of the $PINK1^{Q178X/Q178X}$ medaka is in marked contrast with the more prominent phenotypes of PINK1-depleted zebrafish and *D. melanogaster*. In zebrafish, the Morpholino-mediated suppression of PINK1 caused developmental disorders as well as neurodegeneration (Anichtchik et al., 2008). This severe phenotype of PINK1-depleted zebrafish is surprising. The different phenotypes of the two models might be attributable to the difference of species or strategies. Morpholino may have off-target effect (Ekker and Larson, 2001). On the other hand, non-negligible mutations by ENU may remain although backcross progeny have been analyzed. In *D. melanogaster*, the loss of PINK1 resulted in selective defects in dopaminergic neurons, skeletal muscle, sperm, and mitochondria. It should be noted that the phenotype associated with the loss of PINK1 is distinctly different in model animals such as medaka, zebrafish, mouse, and *D. melanogaster*. The genetic study of *Drosophila* provides compelling evidence that PINK1 works in the same pathway as does parkin. In fact, the loss of function in parkin, $PINK1$, or both genes will result in the same pathology in *Drosophila* (Clark et al., 2006; Park et al., 2006; Yang et al., 2006). An important question that needs to be solved in near future is whether the genetic relationship demonstrated in *Drosophila* is also observed in other PD model animals, including medaka.

Diffuse signal pattern of medaka $PINK1$ mRNA in the gray matter is consistent with that of rat and mouse $PINK1$ (Taymans et al., 2006). The distribution of $PINK1$ mRNA is not restricted to the dopaminergic neurons in rat, mouse and our medaka fish. This makes it difficult to explain why loss of PINK1 function leads to the dysfunctions of dopaminergic neurons. The ways to prove the
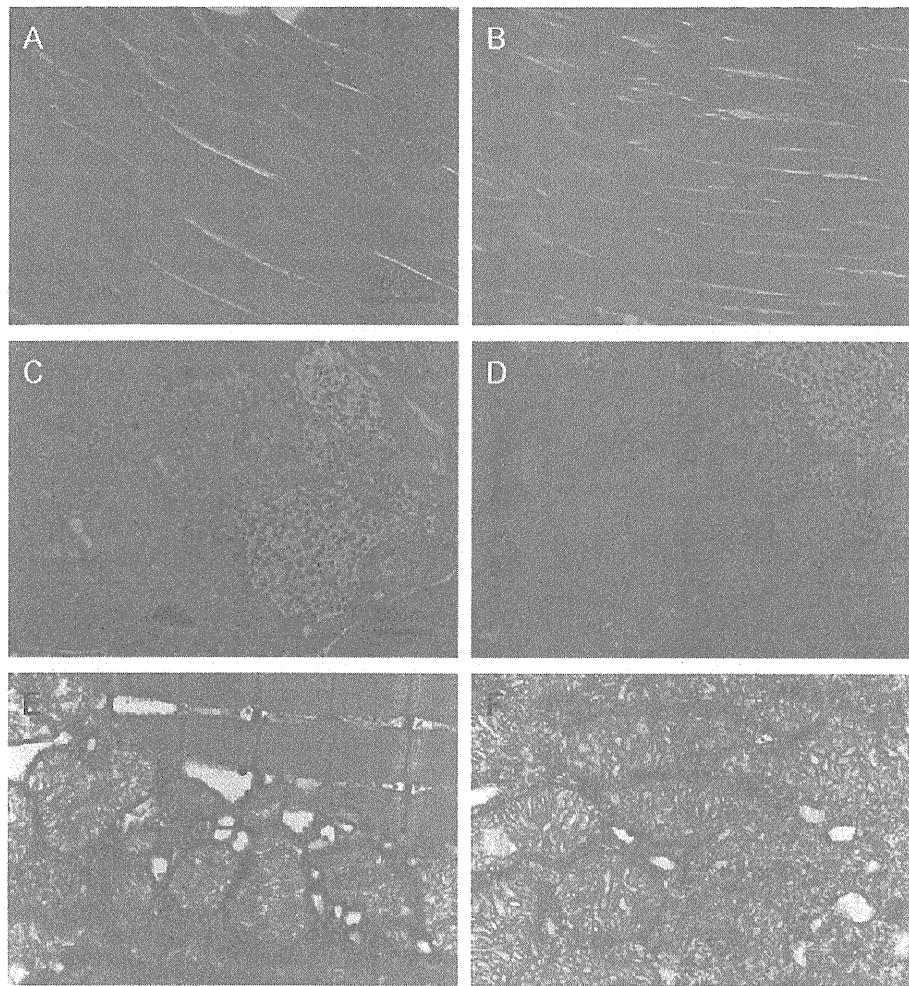
18   H. Matsui et al. / Neuroscience Research xxx (2009) xxx–xxx

Fig. 6. Histological analysis of muscle and testes in $PINK1^{Q178X/Q178X}$ medaka fish (12 months). (A, C, and E) PINK1$^{WT/WT}$. (B, D, and F) $PINK1^{Q178X/Q178X}$. (A and B) Hematoxilin–eosin staining of the muscle. (C and D) Toluidine blue staining of the testes. (E and F) Electron-microscopic image of mitochondria in the muscle. (A–F) Muscles, testes and mitochondria are intact in the $PINK1^{Q178X/Q178X}$ medaka. (F) Altered cristae morphology, fragmentation or elongation of mitochondria were not detected. (For interpretation of the references to color in this figure legend, the reader is referred to the web version of the article.)
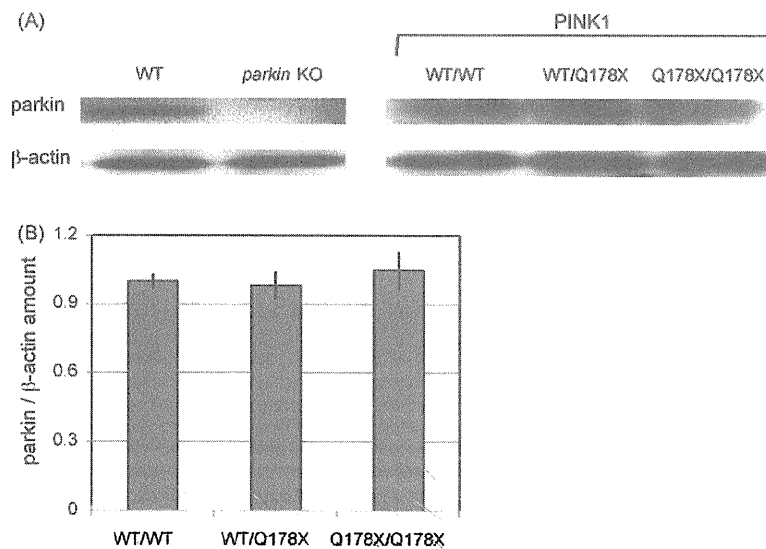

Fig. 7. Amount of parkin protein in $PINK1^{Q178X/Q178X}$ medaka (18 months). (A) Amount of protein in medaka parkin examined by Western blot analysis. (B) Ratio of parkin/β-actin (loading control) for each genotype (average amount for $PINK1^{WT/WT}$ medaka = 1). The amount of parkin does not differ across genotypes (n = 6 for each group).

Please cite this article in press as: Matsui, H., et al., Loss of PINK1 in medaka fish (*Oryzias latipes*) causes late-onset decrease in spontaneous movement. Neurosci. Res. (2009), doi:10.1016/j.neures.2009.10.010
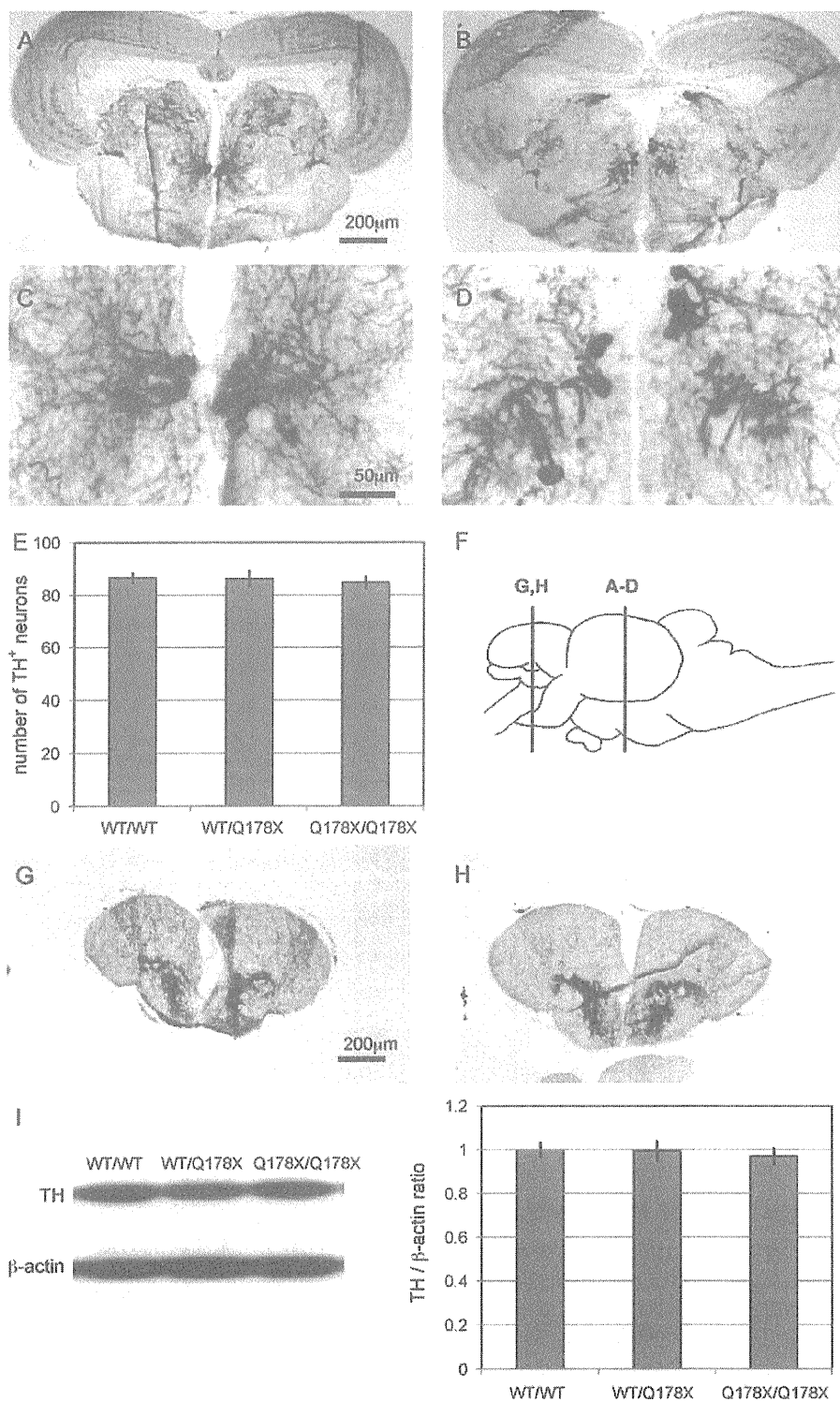
Fig. 8. Immunohistochemistry of tyrosine-hydroxylase and Western blot analysis of $PINK1^{Q178X/Q178X}$ medaka. Coronal sections of striatum and middle diencephalon. (A–D) Representative photographs of middle diencephalic dopaminergic neurons in $PINK1^{WT/WT}$ (A and C) and $PINK1^{Q178X/Q178X}$ (B and D) medaka at 18 months. (E) The number of tyrosine-hydroxylase positive (TH⁺) neurons does not differ across genotypes ($n = 10$ for each group). (G) Striatum dopaminergic fibers for $PINK1^{WT/WT}$ and (H) $PINK1^{Q178X/Q178X}$ medaka at 18 months. The striatum of the $PINK1^{Q178X/Q178X}$ medaka is indistinguishable from that of $PINK1^{WT/WT}$. (F) Map of medaka brain; A–F indicate the section levels of A–D, F and G. (I) Amount of TH protein in the whole brain at 18 months, examined by Western blot analysis and normalized by β-actin (loading control). The graph shows the ratio of tyrosine-hydroxylase (TH)/β-actin for each genotype (average amount for $PINK1^{WT/WT}$ medaka = 1). The amount of TH does not differ across genotypes ($n = 6$ for each group).
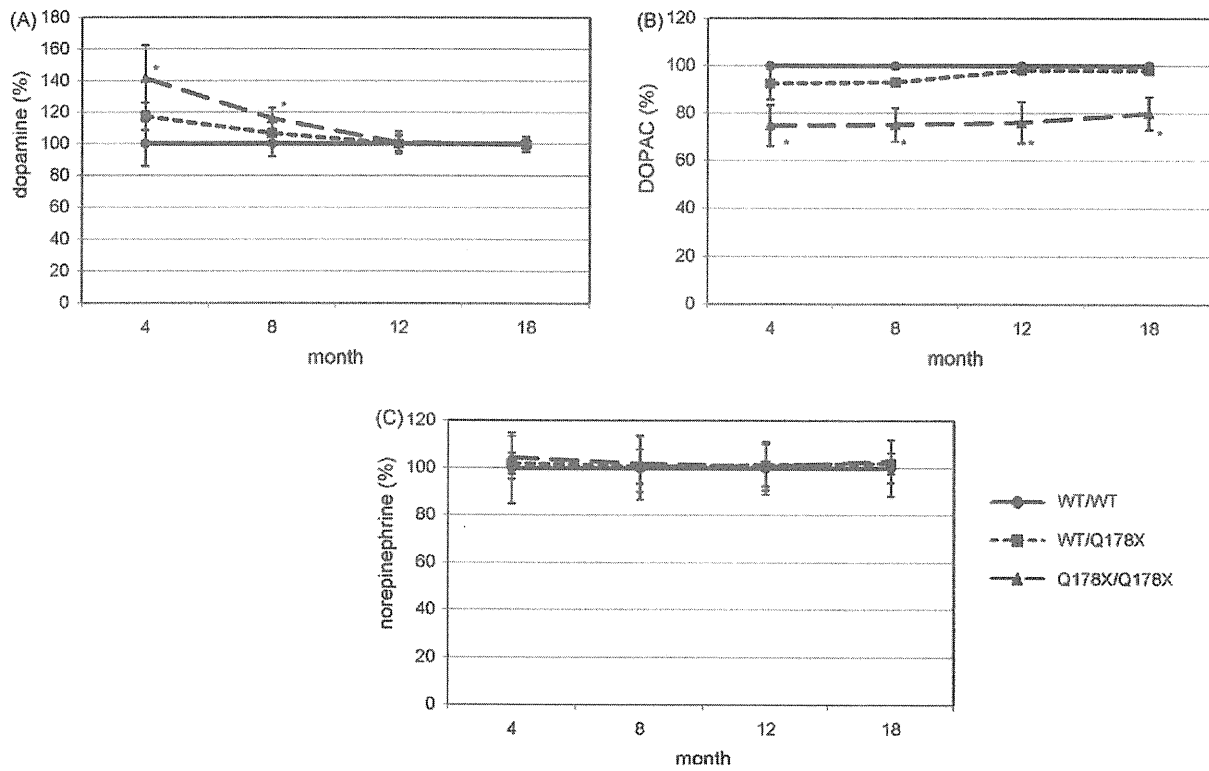
Fig. 9. Amount of dopamine, DOPAC, and norepinephrine in the brain of $PINK1^{Q178X/Q178X}$ medaka. All values are expressed as a percentage of the amount (ng) per protein weight (mg) for $PINK1^{WT/WT}$ ($n = 10$ for each group). (A) The amount of dopamine in the $PINK1^{Q178X/Q178X}$ medaka brain was higher at 4 and 8 months, then registered as normal at 12 and 18 months. (B) The amount of DOPAC decreased at every stage examined. (C) The amount of norepinephrine in the $PINK1^{Q178X/Q178X}$ medaka brain was comparable to that in $PINK1^{WT/WT}$. $^*p < 0.05$ vs. $PINK1^{WT/WT}$.
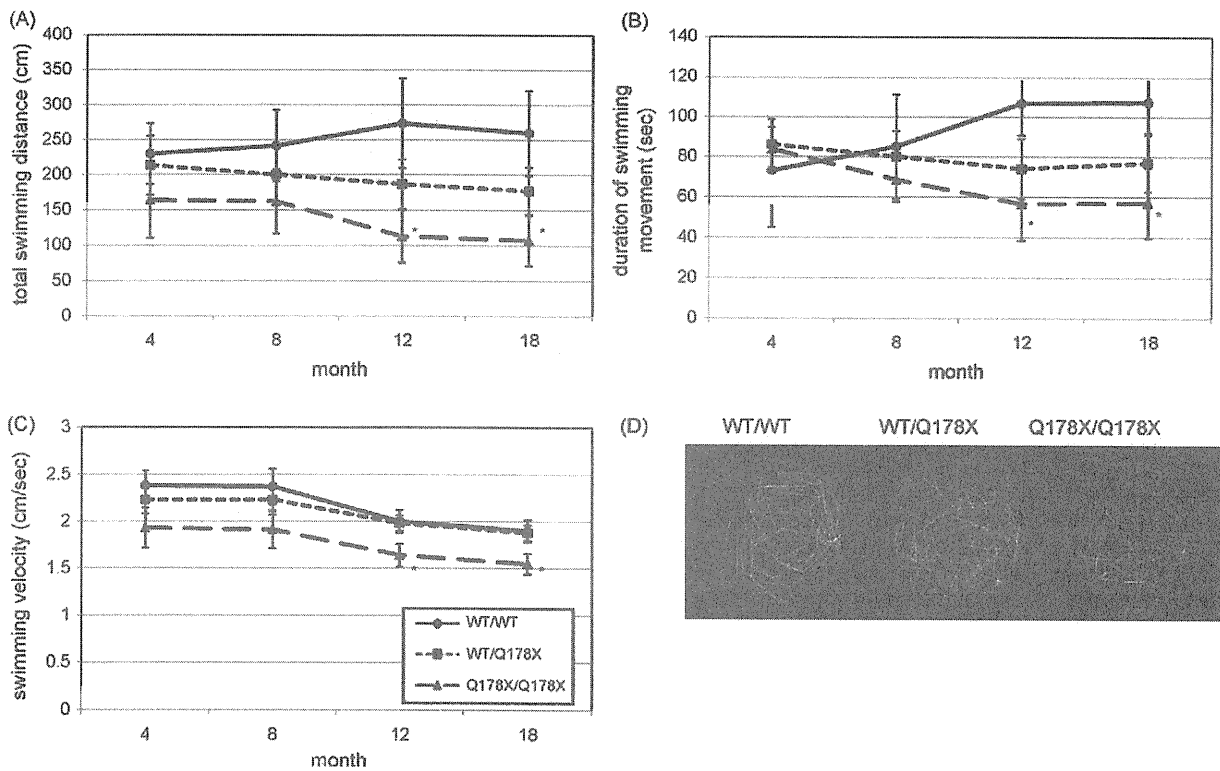

Fig. 10. Spontaneous swimming movement for $PINK1^{Q178X/Q178X}$ medaka. (A) Total swimming distance (cm). (B) Duration of swimming movement (s). (C) Swimming velocity (cm/s). (D) Representative tracks for each genotype. Each genotype showed comparable movement at 4 and 8 months. All parameters for the $PINK1^{Q178X/Q178X}$ medaka decreased at 12 and 18 months ($n = 15$ for each group). $^*p < 0.05$ vs. $PINK1^{WT/WT}$.

genotype–phenotype relationship include complementing the putative causal allele *in vivo* or *in vitro* by transgenesis or retroviral transduction, non-complementation of a null allele generated by homologous recombination, or backcrossing for many generations to the outcross strain (Cook et al., 2006). Therefore, we conducted the overall experiments using not only 4–6 times back-crossed fish but also fish back-crossed more than 7 times. They all showed the same results, suggesting that loss of PINK1 function indeed resulted in the phenotypes shown in this manuscript. However, we analyzed only a single line of *PINK1* mutant and did not perform rescue experiments using transgenic medaka fish in this study. Therefore further experiments are necessary to elucidate the genotype–phenotype relationship.

In conclusion, this report reveals a new *in vivo* function for PINK1. PINK1 affects the metabolism of dopamine in the brain long before the loss of dopaminergic neurons. PINK1-deficient medaka exhibited decreased spontaneous movement only at the late-adult stage, a phenotype that recapitulates a typical symptom of PD. We recently generated another PD model by treating fish with a chemical neurotoxin, MPTP, a standard method used to induce PD (Matsui et al., 2009). The treatment indeed induced the loss of dopaminergic cells and movement disorder. The medaka PD models can therefore contribute significantly to our understanding of the molecular mechanisms underlying the pathology of PD.

References

Anichtchik, O., Diekmann, H., Fleming, A., Roach, A., Goldsmith, P., Rubinsztein, D.C., 2008. Loss of PINK1 function affects development and results in neurodegeneration in zebrafish. J. Neurosci. 28, 8199–8207.

Blum, D., Torch, S., Lambeng, N., Nissou, M., Benabid, A.L., Sadoul, R., Verna, J.M., 2001. Molecular pathways involved in the neurotoxicity of 6-OHDA, dopamine and MPTP: contribution to the apoptotic theory in Parkinson's disease. Prog. Neurobiol. 65, 135–172.

Clark, I.E., Dodson, M.W., Jiang, C., Cao, J.H., Huh, J.R., Seol, J.H., Yoo, S.J., Hay, B.A., Guo, M., 2006. *Drosophila* pink1 is required for mitochondrial function and interacts genetically with parkin. Nature 441, 1162–1166.

Cook, M.C., Vinuesa, C.G., Goodnow, C.C., 2006. ENU-mutagenesis: insight into immune function and pathology. Curr. Opin. Immunol. 18, 627–633.

Ekker, S.C., Larson, J.D., 2001. Morphant technology in model developmental systems. Genesis 30, 89–93.

Exner, N., Treske, B., Paquet, D., Holmström, K., Schiesling, C., Gispert, S., Carballo-Carbajal, I., Berg, D., Hoepken, H.H., Gasser, T., Krüger, R., Winklhofer, K.F., Vogel, F., Reichert, A.S., Auburger, G., Kahle, P.J., Schmid, B., Haass, C., 2007. Loss-of-function of human PINK1 results in mitochondrial pathology and can be rescued by parkin. J. Neurosci. 27, 12413–12418.

Gandhi, S., Muqit, M.M., Stanyer, L., Healy, D.G., Abou-Sleiman, P.M., Hargreaves, I., Heales, S., Ganguly, M., Parsons, L., Lees, A.J., Latchman, D.S., Holton, J.L., Wood, N.W., Revesz, T., 2006. PINK1 protein in normal human brain and Parkinson's disease. Brain 129, 1720–1731.

Gasser, T., 2005. Genetics of Parkinson's disease. Curr. Opin. Neurol. 18, 363–369.

Haque, M.E., Thomas, K.J., D'Souza, C., Callaghan, S., Kitada, T., Slack, R.S., Fraser, P., Cookson, M.R., Tandon, A., Park, D.S., 2008. Cytoplasmic Pink1 activity protects neurons from dopaminergic neurotoxin MPTP. Proc. Natl. Acad. Sci. U.S.A. 105, 1716–1721.

Hatano, Y., Li, Y., Sato, K., Asakawa, S., Yamamura, Y., Tomiyama, H., Yoshino, H., Asahina, M., Kobayashi, S., Hassin-Baer, S., Lu, C.S., Ng, A.R., Rosales, R.L., Shimizu, N., Toda, T., Mizuno, Y., Hattori, N., 2004. Novel PINK1 mutations in early-onset parkinsonism. Ann. Neurol. 56, 424–427.

Hedrich, K., Hagenah, J., Djarmati, A., Hiller, A., Lohnau, T., Lasek, K., Grünewald, A., Hilker, R., Steinlechner, S., Boston, H., Kock, N., Schneider-Gold, C., Kress, W., Siebner, H., Binkofski, F., Lencer, R., Münchau, A., Klein, C., 2006. Clinical spectrum of homozygous and heterozygous PINK1 mutations in a large German family with Parkinson disease: role of a single hit? Arch. Neurol. 63, 833–838.

Kitada, T., Asakawa, S., Hattori, N., Matsumine, H., Yamamura, Y., Minoshima, S., Yokochi, M., Mizuno, Y., Shimizu, N., 1998. Mutations in the parkin gene cause autosomal recessive juvenile parkinsonism. Nature 392, 605–608.

Kitada, T., Pisani, A., Porter, D.R., Yamaguchi, H., Tscherter, A., Martella, G., Bonsi, P., Zhang, C., Pothos, E.N., Shen, J., 2007. Impaired dopamine release and synaptic plasticity in the striatum of PINK1-deficient mice. Proc. Natl. Acad. Sci. U.S.A. 104, 11441–11446.

Matsui, H., Taniguchi, Y., Inoue, H., Uemura, K., Takeda, S., Takahashi, R., 2009. A chemical neurotoxin, MPTP induces Parkinson's disease like phenotype, movement disorders and persistent loss of dopamine neurons in the medaka fish (*Oryzias latipes*). Neurosci. Res. 65, 263–271.

Park, J., Lee, S.B., Lee, S., Kim, Y., Song, S., Kim, S., Bae, E., Kim, J., Shong, M., Kim, J.M., Chung, J., 2006. Mitochondrial dysfunction in Drosophila PINK1 mutants is complemented by parkin. Nature 441, 1157–1161.

Pridgeon, J.W., Olzmann, J.A., Chin, L.S., Li, L., 2007. PINK1 protects against oxidative stress by phosphorylating mitochondrial chaperone TRAP1. PLoS Biol. 19, e172.

Sim, C.H., Lio, D.S., Mok, S.S., Masters, C.L., Hill, A.F., Culvenor, J.G., Cheng, H.C., 2006. C-terminal truncation and Parkinson's disease-associated mutations down-regulate the protein serine/threonine kinase activity of PTEN-induced kinase-1. Hum. Mol. Genet. 15, 3251–3262.

Tan, E.K., Yew, K., Chua, E., Puvan, K., Shen, H., Lee, E., Puong, K.Y., Zhao, Y., Pavanni, R., Wong, M.C., Jamora, D., de Silva, D., Moe, K.T., Woon, F.P., Yuen, Y., Tan, L., 2006. PINK1 mutations in sporadic early-onset Parkinson's disease. Mov. Disord. 21, 789–793.

Taniguchi, Y., Takeda, S., Furutani-Seiki, M., Kamei, Y., Todo, T., Sasado, T., Deguchi, T., Kondoh, H., Mudde, J., Yamazoe, M., Hidaka, M., Mitani, H., Toyoda, A., Sakaki, Y., Plasterk, R.H., Cuppen, E., 2006. Generation of medaka gene knockout models by target-selected mutagenesis. Genome Biol. 7, R116.

Taymans, J.M., Van den Haute, C., Baekelandt, V., 2006. Distribution of PINK1 and LRRK2 in rat and mouse brain. J. Neurochem. 98, 951–961.

Unoki, M., Nakamura, Y., 2001. Growth-suppressive effects of BPOZ and EGR2, two genes involved in the PTEN signaling pathway. Oncogene 20, 4457–4465.

Valente, E.M., Abou-Sleiman, P.M., Caputo, V., Muqit, M.M., Harvey, K., Gispert, S., Ali, Z., Del Turco, D., Bentivoglio, A.R., Healy, D.G., Albanese, A., Nussbaum, R., González-Maldonado, R., Deller, T., Salvi, S., Cortelli, P., Gilks, W.P., Latchman, D.S., Harvey, R.J., Dallapiccola, B., Auburger, G., Wood, N.W., 2004. Hereditary early-onset Parkinson's disease caused by mutations in PINK1. Science 304, 1158–1160.

Wood-Kaczmar, A., Gandhi, S., Yao, Z., Abramov, A.S., Miljan, E.A., Keen, G., Stanyer, L., Hargreaves, I., Klupsch, K., Deas, E., Downward, J., Mansfield, L., Jat, P., Taylor, J., Heales, S., Duchen, M.R., Latchman, D., Tabrizi, S.J., Wood, N.W., 2008. PINK1 is necessary for long term survival and mitochondrial function in human dopaminergic neurons. PLoS ONE 3, e2455.

Yang, Y., Gehrke, S., Imai, Y., Huang, Z., Ouyang, Y., Wang, J.W., Yang, L., Beal, M.F., Vogel, H., Lu, B., 2006. Mitochondrial pathology and muscle and dopaminergic neuron degeneration caused by inactivation of *Drosophila* Pink1 is rescued by parkin. Proc. Natl. Acad. Sci. U.S.A. 103, 10793–10798.

Zhou, H., Falkenburger, B.H., Schulz, J.B., Tieu, K., Xu, Z., Xia, X.G., 2007. Silencing of the Pink1 gene expression by conditional RNAi does not induce dopaminergic neuron death in mice. Int. J. Biol. Sci. 3, 242–250.

PI3K inhibition causes the accumulation of ubiquitinated presenilin 1 without affecting the proteasome activity

Nobuhisa Aoyagi [a], Kengo Uemura [a,*], Akira Kuzuya [a], Takeshi Kihara [b], Jun Kawamata [a], Shun Shimohama [c], Ayae Kinoshita [d], Ryosuke Takahashi [a]

[a] Department of Neurology, Kyoto University Graduate School of Medicine, Kyoto, Japan
[b] Department of Neuroscience for Drug Discovery, Graduate School of Pharmaceutical Sciences, Kyoto University, Kyoto, Japan
[c] Department of Neurology, School of Medicine, Sapporo Medical University, Kyoto, Japan
[d] School of Health Sciences, Faculty of Medicine, Kyoto University, Kyoto, Japan

ARTICLE INFO

ABSTRACT

γ-Secretase is an enzymatic complex, composed of presenilin 1 (PS1), nicastrin, pen-2, and aph-1, and is responsible for the intramembranous cleavage of various type-I membrane proteins. The level of each component is tightly regulated in a cell via proteasomal degradation. On the other hand, it has previously been reported that PS1/γ-secretase is involved in the activation of phosphatidylinositol-3 kinase/Akt (PI3K/Akt) pathway. PI3K is inhibited in Alzheimer's disease (AD) brain, whereas the effects of PI3K inhibition on the metabolism of PS1/γ-secretase have not been elucidated. Here, we demonstrate that the treatment of neurons with PI3K inhibitors leads to increased levels of PS1/γ-secretase components through an inhibitory effect on their degradation. Moreover, PI3K inhibition accelerated ubiquitination of PS1. We further show the evidence that the PS1 ubiquitination after PI3K inhibition is represented by the multiple mono-ubiquitination, instead of poly-ubiquitination. Accordingly, treatment of cells with PI3K inhibitor led to a differential intracellular redistribution of PS1 from the one observed after the proteasomal inhibition. These results suggest that PI3K inhibition may trigger the multiple mono-ubiquitination of PS1, which precludes the degradation of PS1/γ-secretase through the proteasomal pathway. Since PS1/γ-secretase is deeply involved in the production of Aβ protein, a deeper knowledge into its metabolism could contribute to a better elucidation of AD pathogenesis.

© 2009 Elsevier Inc. All rights reserved.

Introduction

A major component of the amyloid plaque core in Alzheimer's disease (AD) is the amyloid β peptide (Aβ). γ-Secretase is a protein complex, composed of presenilin 1 or 2 (PS1 or 2), nicastrin, pen-2, and aph-1 and is responsible for the production of Aβ [5,7,9,21]. Recent reports demonstrated that the levels of these four components are tightly regulated each other and, thus, down-regulation of one of these components leads to a decreased level of the whole complex [20]. All of these γ-secretase components can be degraded through the ubiquitin–proteasome system [3,10,11,13,18]. Upon conjugation of polyubiqutin chains to target proteins, proteasome can degrade various proteins including misfolded or aggregated proteins [8,12,24]. On the other hand, multiple mono-ubiquitination of proteins has been attributed to other cellular functions, such as protein trafficking and endocytosis [1,19].

PS1 is a causative gene for familial AD and is considered to be the catalytic core of γ-secretase [6,17,26]. In addition to the well-established role in γ-secretase activity, many reports have shown that PS1 is involved in the activation of phosphatidylinositol-3 kinase/Akt (PI3K/Akt) pathway [2,25], thereby suppressing the activity of glycogen synthase kinase-3β (GSK-3β). Conversely, abnormal activities of GSK-3β have been reported in AD brains [4], indicating that PI3K/Akt pathway is inhibited in AD. Although PS1 has recently been demonstrated to be one of GSK-3β substrates [14,22,23], the effect of PI3K/Akt inhibition on the metabolism of PS1/γ-secretase components has not been demonstrated, yet. To elucidate how PI3K/Akt affects the metabolism of PS1/γ-secretase, we treated mouse primary neurons with PI3K/Akt inhibitors and analyzed their effects on the metabolism of PS1/γ-secretase.

Materials and methods

Cell culture and drug treatment. Primary neurons were obtained from the cerebral cortex of fetal ICR mice (14 days gestation) and cultured in Neurobasal medium supplemented with B27

* Corresponding author. Address: Department of Neurology, Kyoto University School of Medicine, 54 Kawahara-Cho, Shogo-In, Sakyo-Ku, Kyoto 606-8397, Japan. Fax: +81 75 751 9541.
E-mail address: ueken@kuhp.kyoto-u.ac.jp (K. Uemura).

(Invitrogen). Neurons in culture day from 10 to 12 were used for the experiment. HEK293 cells were maintained in Dulbecco's modified Eagle's medium containing 10% fetal bovine serum. For PI3K inhibition, cells were treated with either LY294002 or Wortmannin diluted in the media to give a final concentration of 5 μM and 50 nM, respectively, for an indicated period of time. For the inhibition of Akt, cells were treated with 1 μM Akt inhibitor IV. For proteasome inhibition, cells were treated with 1 μM lactacystin. For inhibition of protein synthesis, cells were treated with 5 μg/mL cycloheximide. Control cells were treated with Dimethylsulfoxide (DMSO).

Construction of plasmids expressing presenilin 1 and ubiquitin mutants and transient transfection. Creation of wild-type human PS1 plasmid was described elsewhere [23]. Human wild-type ubiquitin cDNA with a hemagglutinin (HA) tag (HA-WT-Ub) and HA-tagged ubiquitin whose all lysine residues were replaced with arginine (HA-K0-Ub) were generous gifts from Dr. Y. Imai (Tohoku University). Precise cloning of all reading frames was verified by direct sequencing. Lipofectamine LTX agent (Invitrogen) was used for transient transfection in HEK293 cells according to the manual.

Antibodies and chemical reagents. Rabbit polyclonal anti-PS1 N-terminal fragment (NTF) antibody was from Santa Cruz. Rabbit polyclonal anti-Ubiquitin antibody was from DAKO. Mouse monoclonal anti-PS1 C-terminal fragment (CTF) was from Chemicon. Rabbit polyclonal Anti-nicastrin, mouse monoclonal anti-β-actin, mouse monoclonal anti-β-tubulin, mouse monoclonal anti-γ-tubulin antibodies were from Sigma. Rabbit polyclonal Anti-aph-1 antibody was from Affinity BioReagents. Rat monoclonal Anti-HA tag antibody was from Roche. Donkey polyclonal Anti-mouse and rabbit horseradish peroxidase-conjugated secondary antibodies were from Amersham Biosciences. For immunostaining, Alexa Fluor 546 goat anti-mouse IgG (H + L) conjugate and Alexa Fluor 488 goat anti-rabbit IgG (H + L) conjugate from Molecular Probes were used as secondary antibodies. LY294002 and Wortmannin were from Sigma. AKT inhibitor IV was from Merck. DMSO was from Nacalai Tesque. Lactacystin was from Kyowa Medex. Cycloheximide was from Calbiochem.

Western blotting and immunoprecipitation. The protein levels of γ-secretase components were analyzed by Western blotting as described previously [23]. For immunoprecipitation, cells were washed and scraped like above. NP40 soluble fractions were made by solubilizing the samples in TNE Buffer containing 10 mM Tris–HCl (pH 7.8), 150 mM NaCl, 1% NP40, 1 mM EDTA with proteinase inhibitor cocktail (Roche). Remnant pellets were then further solubilized in TNE buffer plus 1% SDS. After 10-fold dilution of SDS in SDS-free TNE buffer, the samples were subjected to immunoprecipitation. Alternatively, TNE Buffer plus 1% SDS was directly used for cell lysis. Cell lysates containing 1% SDS were diluted 10-fold in SDS-free TNE buffer before immunoprecipitation to avoid degeneration of immunoglobulins. The samples were pretreated with Protein G-Sepharose (GE Healthcare Lifesciences) for an hour at 4 °C to reduce nonspecific binding. After centrifugation, supernatants were collected and precipitating antibodies were added. The samples were rotated at 4 °C for an hour, followed by the addition of new Protein G-Sepharose and rotation for another hour at 4 °C. Immune complexes were washed five times with TNE Buffer. Sample buffer was added to the immune complexes and incubated at room temperature for 10 min. The immunoprecipitated proteins were subjected to SDS–PAGE.

Semi-quantitative reverse transcriptase- polymerase-chain reaction. Total RNA was extracted from primary cultured neurons using ISOGEN (Nippon Gene) and the concentration of RNA was measured by Bio-rad SmartSpec Plus spectrophotometer. The same amount of total RNA was processed for cDNA synthesis using oligo (dT) primers and reverse transcriptase, using TaKaRa RNA LA PCR Kit (AMV) (TaKaRa, Tokyo, Japan). The resulting cDNA was ampli-

fied by polymerase-chain reaction. The primers used were 5′-GGT ACCCAAGAACCCCAAGT-3′ and 5′-CCGGGTCTTCACTCGTTAGA-3′ for mouse presenilin 1, 5′-GGAACCAACTTCAGCAGCTC-3′ and 5′-GAGCCTCTCTGTCCTGTTGG-3′ for mouse nicastrin, 5′-ACCACAGTCC ATGCCATCAC-3′ and 5′-TCCACCACCCTGTTGCTGTA-3′ for mouse GAPDH. The number of cycle was optimized so as to avoid saturation of amplified DNA as previously described [15].

Proteasome activity assay. Proteasome activity was quantified by the measurement of the release of 7-amino-4-methylcoumarin from the fluorogenic peptide Suc-Leu-Leu-Val-Tyr-7-amino-4-methylcoumarin (Suc-LLVY-AMC, Affinity Research Product). Primary cultured neurons were washed twice with phosphate-buffered saline (PBS), harvested on ice, and resuspended into a buffer containing 25 mM Hepes and 0.5 mM EDTA. Cells were centrifuged and lysed by brief sonication. SDS solution was added to the lysate to give the final concentration of 0.03%. Then the fluorogenic substrate Suc-Leu-Leu-Val-Tyr-7-amino-4-methylcoumarin was added to the mixture and incubated at 37 °C for 30 min. Proteasome activity was detected by changes in fluorescence intensity at 355 nm of excitation and 460 nm of emission using an automatic multi-well plate reader. The relative activity was standardized by protein concentration, which was determined using BCA protein assay kit (Pierce).

Immunostaining. Cells were fixed with 4% paraformaldehyde for 20 min. Fixed cells were blocked with 3% BSA in PBS with 0.2% Triton X-100 for 15 min and incubated overnight at 4 °C with each antibody diluted in PBS containing 3% BSA. Immunoreactivity was visualized using the species-specific secondary antibodies mentioned above. Samples were examined using a LSM (Zeiss) confocal scanning microscope.

Statistical analysis. The relative density of the bands in Western blotting was analyzed by quantitative densitometry using a computerized image analysis program (NIH image 1.59). To compare the ratios of each γ-secretase component to β–actin between treatments, Student's t-test was used for the analysis. The mRNA levels of γ-secretase components and the proteasomal activity were analyzed by using One-way Factorial ANOVA, followed by post hoc Fisher's protected least significant difference. Quantified data were expressed as the means ± SD, and significance was assessed at $P < 0.05$.

Results and discussion

We first investigated the effect of PI3K/Akt activity on the metabolism of γ-secretase. To test this, primary cultured mouse neurons were treated with either vehicle (DMSO) or a PI3K inhibitor, LY294002 for 48 h. Immunoblotting of the cell lysate demonstrated increased levels of γ-secretase components (PS1, nicastrin, Pen-2, Aph-1) upon PI3K inhibition (Fig. 1A, left). The quantitative analysis of each γ-secretase component band intensity revealed significant increase after the LY294002 treatment (Fig. 1A, right, $n = 3$, $p < 0.05$). Similarly, inhibition of Akt activity by a treatment with Akt inhibitor IV for 24 h caused an accumulation of γ-secretase complex components (Fig. 1B). The statistical analysis of three independent experiments showed a significant increase of every γ-secretase component after Akt inhibition ($p < 0.05$, data not shown), validating the involvement of PI3K/Akt pathway in the regulation of γ-secretase components protein levels.

We then asked whether this accumulation is due to an accelerated transcription of γ-secretase components or, alternatively, an inhibition on the degradation machinery of the components. To answer this question, we analyzed the mRNA levels of γ-secretase components (PS1 and nicastrin) under PI3K inhibition by semi-quantitative RT-PCR. Mouse primary cultured neurons were treated with either vehicle or one of PI3K inhibitors (Wortmannin or LY294002) for 24 h. Total mRNA was extracted from the cell
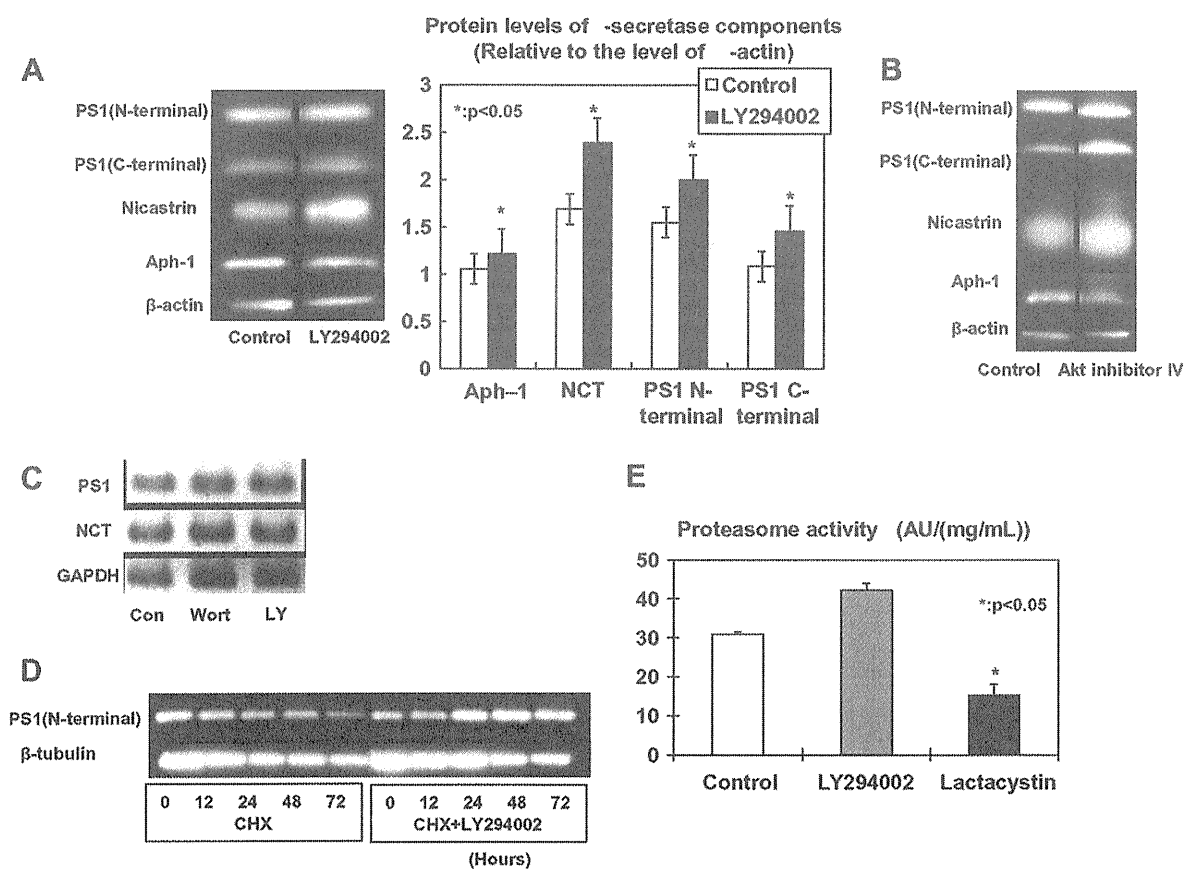
Fig. 1. The level of PS1/γ-secretase complex increases upon an inhibition of PI3K/Akt pathway (A) Mouse cortical neurons in primary culture were treated with either vehicle (DMSO) or LY294002 for 48 h. The cells were collected and cell lysates were subjected to immunoblotting by anti-PS1 (N-terminal, C-terminal), Nicastrin, Aph-1, or β-actin antibodies (left). The band intensity of each γ-secretase component is normalized by that of β-actin and analyzed by Student's t-test. The level of each component was significantly higher in the cells treated with LY294002 compared to that in the cells treated with vehicle (right, n = 3, p < 0.05). (B) Mouse cortical neurons in primary culture were treated with either vehicle (DMSO) or AKT inhibitor IV for 24 h. Cells were collected and immunoblotted with antibodies against anti-PS1 (N-terminal, C-terminal), Nicastrin, Aph-1, or β-actin. (C) Mouse cortical neurons in primary culture were treated with vehicle, Wortmannin or LY294002 for 24 h. Cells were collected and the total RNA was extracted from the cell lysates. mRNA levels were semi-quantified by RT-PCR. The mRNA levels of γ-secretase components was normalized to that of GAPDH and analyzed by One-way Factorial ANOVA (n = 3). (D) Mouse cortical neurons in primary culture were treated with CHX alone or CHX together with LY294002. Cells were collected 0. 12, 24, 48, 72 h after the treatment. Cell lysates were subjected to immunoblotting by anti-PS1 antibody. The expression level of PS 1 decreased along with the time after CHX treatment. Co-treatment of cells with CHX and LY294002 inhibited the decrease of PS1. β-tubulin levels were consecutively decreased after CHX treatment regardless of the presence of LY294002. (E) Primary culture neurons were treated with vehicle, LY294002 or lactacystin for 24 h. Proteasomal activity defined by release of 7-amino-4-methylcoumarin from the fluorogenic peptide Suc-Leu-Leu-Val-Tyr-7-amino-4-methylcoumarin was measured by fluorescence intensity. Only lactacystin treatment showed significant decrease in proteasome activity (n = 3, One-way Factorial ANOVA).

pellets, followed by the RT-PCR analyses of PS1, nicastrin and β-actin mRNA levels (Fig. 1C). We observed no significant difference between the vehicle and a PI3K inhibitor (Wortmannin or LY294002) treatment groups with respect to the mRNA levels of PS1 and nicastrin (n = 3). These results indicate that the transcriptions of PS1 and nicastrin were not affected by PI3K inhibition.

We then examined whether PI3K inhibition cause an altered degradation activity of PS1 in neurons, using a protein synthesis inhibitor, cycloheximide (CHX). Mouse primary cultured neurons were incubated with CHX in the presence or absence of LY294002 for 0, 12, 24, 48, 72 h. The protein levels of PS1 and β-tubulin gradually decreased by the treatment with CHX alone, reflecting the protein degradation in the absence of new protein synthesis (Fig. 1D, top, left). On the contrary, simultaneous treatment of cells with CHX and LY294002 maintained the amount of PS1 up to 72 h after the treatment (Fig. 1D, top, right). These results indicate that PI3K inhibition precludes the degradation of PS1 to stabilize its protein expression. Conversely, the decrease in cellular β-tubulin levels was comparable between the cells treated with CHX alone and the cells simultaneously treated with CHX and LY294002 (Fig. 1D, bottom), indicating LY294002 specifically stabilize the level of PS1.

In order to rule out a possibility that PI3K inhibition caused general inhibition of proteasome activity, thereby non-specifically inhibiting the degradation of γ-secretase components as well as many other proteins, we measured the proteasome activity within mouse primary cultured neurons under PI3K inhibition. Mouse primary cultured neurons were treated with vehicle, LY294002, or lactacystin, a specific proteasome inhibitor, for 24 h followed by the measurement of proteasome activity (Fig. 1E). There was no significant difference in proteasome activity between in the cells treated with the vehicle and LY294002, whereas significant decrease in proteasome activity was observed in the cells treated with lactacystin. Thus, LY294002 stabilizes PS1/γ-secretase components by specifically inhibiting their degradation.

Since the level of PS1 is regulated by the ubiquitin–proteasome system [13,18], we postulated that PI3K inhibition could have altered the ubiquitination status of PS1, thereby stabilizing its protein level. To test this, HEK293 cells were transfected with wild-type PS1 and treated with either PI3K inhibitors (Wortmannin or LY294002) or proteasome inhibitor (lactacystin). After the treatment, cell lysates were fractionated into NP40 soluble or insoluble fractions. Each fraction was immunoprecipitated with anti-PS1 antibody, followed by Western blotting with anti-ubiquitin

	1	2	3	4	5	6
Transfect	—	PS1	PS1	PS1	PS1	PS1
Treat.	—	—	—	Wort	LY	Lacta
IP	IgG	IgG	PS1	PS1	PS1	PS1

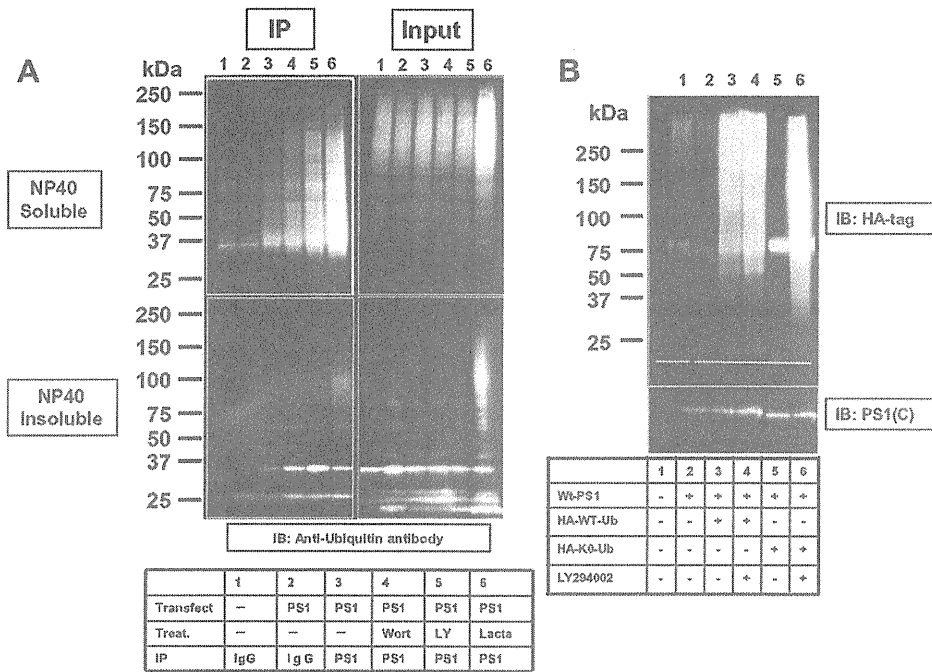|	1	2	3	4	5	6
Wt-PS1	-	+	+	+	+	+
HA-WT-Ub	-	-	+	+	-	-
HA-K0-Ub	-	-	-	-	+	+
LY294002	-	-	-	+	-	+

Fig. 2. PI3K inhibition increases multiple mono-ubiquitination of PS1. (A) HEK293 cells were transfected with wild-type PS1 and treated with either PI3K inhibitors (Wortmannin or LY294002) or a proteasome inhibitor (lactacystin). After the treatment, cell lysates were fractionated into NP40 soluble or insoluble fractions. Each fraction was immunoprecipitated with anti-PS1 C-terminal antibody, followed by Western blotting with anti-ubiquitin antibody. Treatment with Wortmannin, LY294002, and lactacystin increased ubiquitinated protein in the immunoprecipitates from NP40 soluble fraction (Upper left panel). Only lactacystin treatment increased total ubiquitinated protein in the NP40 soluble lysate (Upper right panel). In the NP40 insoluble fraction, only lactacystin treatment increased ubiquitinated proteins both in the immunoprecipitate (bottom left panel) and lysate (bottom right panel). (B) HEK293 cells were transiently co-transfected with wild-type presenilin 1 and with HA-tagged wild-type ubiquitin (HA-WT-Ub) or HA-tagged ubiquitin whose all lysine residues were replaced with arginine (HA-K0-Ub). Cells were treated either with vehicle or LY294002 for 24 h. Cells were harvested and solubilized with 1% SDS to disrupt protein–protein interaction. After dilution of SDS concentration, lysates were immunoprecipitated with anti-PS1 C-terminal antibody. Immunoprecipitates were analyzed by Western blotting using HA-tag antibody. Expression of HA-WT-Ub alone accelerated the ubiquitination of PS1 (3rd lane), which was further enhanced by the treatment with LY294002 (4th lane). The expression of HA-K0-Ub alone did not enhance the ubiquitination of PS1 (5th lane), whereas treatment with LY294002 drastically enhanced the ubiquitination (6th lane).

antibody (Fig. 2A). Interestingly, the ubiquitination of PS1 in the NP40 soluble fraction was enhanced in the cells treated with either of PI3K inhibitors (Wortmannin or LY294002) (Fig. 2A, top left panel, lanes 4 and 5), compared to that in the cells treated with vehicle (Fig. 2A, top left panel, lane 3). Neither Wortmannin nor LY294002 increased total ubiquitinated proteins in the NP40 soluble fraction, and in the insoluble fraction (Fig. 2A, top and bottom right panels, lanes 4 and 5), indicating that proteasome activity itself was not altered by the treatment with these PI3K inhibitors (see also Fig. 1E). On the contrary, lactacystin treatment expectedly increased the level of total ubiquitinated proteins in both soluble and insoluble fractions (Fig. 2A, top and bottom right panels, lane 6), indicating an effective inhibition of proteasome activity by the treatment. Moreover, treatment with PI3K inhibitors did not increase the level of ubiquitinated PS1 in the insoluble fraction (Fig. 2A, bottom left panel, lanes 4 and 5), whereas lactacystin treatment did (Fig. 2A, top left panel, lane 6).

These results suggest that the ubiquitination of PS1 under PI3K inhibition might have different property from that observed under proteasome inhibition. Ubiquitin is first linked to a target protein via covalent bond between its C-terminus glycine residue (G76) and a lysine (K) residue in the target protein. Ubiquitin chain is subsequently achieved by the sequential conjugation of an internal K residue of ubiquitin (i.e. K6, 11, 27, 29, 33, 48, or 63) to the G76 residue of a new ubiquitin. Polyubiquitin chains linked via K48 are typically associated with protein degradation by the proteasome [18,12,24]. On the other hand, multiple mono-ubiquitination, achieved by the addition of multiple monomeric ubiquitin molecules to K residues of target proteins has been attributed to various other cellular functions [1,19].

In order to assess the mode of PS1 ubiquitination in the presence of PI3K inhibitor, HEK293 cells were transiently co-transfected with wild-type PS1 together with either HA-tagged wild-type ubiquitin (HA-WT-Ub) or HA-tagged ubiquitin whose all lysine residues were replaced with arginine (HA-K0-Ub). HA-K0-Ub cannot form covalent bond except for the terminal carboxyl residue, thus considered to represent multiple mono-ubiquitination. Cells were treated with either vehicle or LY294002, followed by the IP-Western blotting to detect ubiquitinated PS1. In order to avoid a possibility that immunoprecipitation with anti-PS1 antibody pulls down PS1-interacting protein together with PS1, which contaminates the 'true' ubiquitination signal of PS1, cells were first lysed with high concentration of SDS to disrupt the protein–protein interaction except for covalent bonds. The lysates were subsequently diluted to be applicable for IP. Expression of HA-WT-Ub alone enhanced the ubiquitination of PS1 in our experimental system, which was further accelerated in the presence of PI3K inhibitor, LY294002 (Fig. 2B). In contrast to the HA-WT-Ub expression, the expression of HA-K0-Ub caused minimal ubiquitination of PS1 in the absence of PI3K inhibition. Surprisingly, treatment with LY294002 markedly increased the ubiquitination of PS1 by the HA-K0-Ub. Although we could not rule out a possibility that the linkage between the K residue of the endogenous ubiquitin and the terminal carboxyl residue of HA-K0-Ub formed polyubiquitin chains under PI3K inhibition, these results suggest that PI3K inhibition could induce multiple mono-ubiquitination of PS1.

Recent studies have shown that ubiquitination acts as a signal for intracellular trafficking in addition to the proteasomal function [1,19]. In order to prove that the PI3K inhibition and the proteasome inhibition drive differential modes of ubiquitination, we
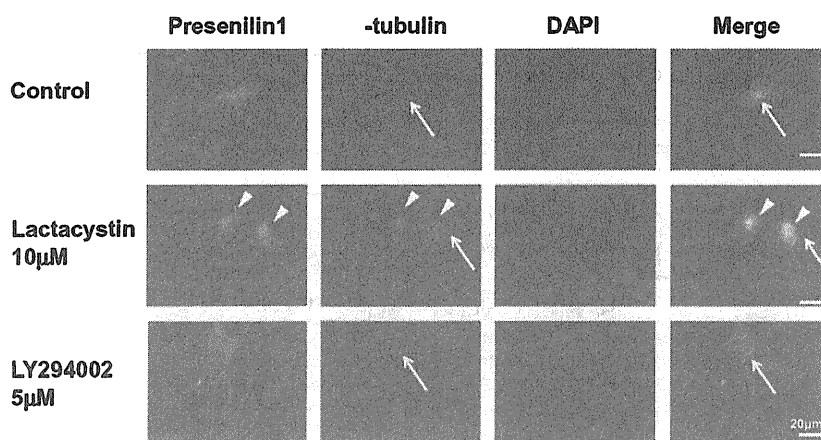
Fig. 3. PI3K inhibition does not cause accumulation of PS1 in the aggresome. Primary neurons were treated with vehicle (DMSO), lactacystin or LY294002. After treatment, cells were immunostained with antibodies against PS1 (green) and γ-tubulin (red). Nucleus was stained with DAPI (blue). In control cells (top panels), PS1 is distributed around the nucleus with minimal co-localization with γ-tubulin, which represents immunoreactivity of a centrosome (arrows). After lactacystin treatment (middle panels), prominent perinuclear co-localization of PS1 and γ-tubulin (arrowheads) around the centrosome (arrows) was observed, indicating the accumulation of PS1 in the aggresome. LY294002 (bottom panels) treatment did not enhance the co-localization of PS1 with γ-tubulin (arrows).

investigated the intracellular localization of PS1 after PI3K, as well as proteasome inhibition. Mouse primary cultured neurons were triply stained with the anti-PS1 antibody, the anti-γ-tubulin antibody and DAPI after vehicle, LY294002 or lactacystin treatment. γ-Tubulin was used as a marker of a centrosome or an aggresome, as previously reported [13]. In control cells, PS1 immunoreactivity was observed mainly in perinuclear area, probably reflecting ER distribution (Fig. 3, top). γ-Tubulin was visualized as a perinuclear spot, representing the distribution of a centrosome (Fig. 3, top, arrows). In cells treated with lactacystin, PS1 was largely colocalized with γ-tubulin in the perinuclear area (Fig. 3, middle panels, arrowheads), indicating the redistribution of PS1 to an aggresome, which was formed around the centrosome (Fig. 3, middle panels, arrows). Interestingly, in cells treated with LY294002, the perinuclear co-localization of PS1 with γ-tubulin was negligible, whereas PS1 was likely to be widely redistributed into the intracellular membranes (Fig. 3C, bottom panels). γ-Tubulin immunoreactivity was similar to that in control cells (Fig. 3C, bottom panels, arrows), reflecting the intracellular distribution of a centrosome. These results suggest that an accelerated ubiquitination of PS1 under PI3K inhibition could alter the intracellular localization of PS1 in a different fashion from that under proteasomal inhibition.

Since PS1/γ-secretase is deeply involved in Aβ production, deeper knowledge into its metabolism under physiological as well as pathological settings is important for investigating the pathogenesis of AD. In the present study, we have demonstrated that PI3K inhibition leads to an accumulation of ubiquitinated PS1. This accelerated ubiquitination after PI3K inhibition was suggested to be different from the proteasome-targeting poly-ubiquitination of PS1, because of following experimental results: (1) Protein levels of PS1/γ-secretase were increased rather than decreased after PI3K inhibition. (2) The mode of ubiquitination was considered to be the multiple mono-ubiquitination rather than the poly-ubiquitination according to the HA-KO-Ub experiment. (3) An accelerated ubiquitination of PS1 after PI3K inhibition led to different intracellular distribution of PS1 from that observed after proteasomal inhibition. Thus, it can be postulated that the multiple-mono-ubiquitination of PS1 after PI3K inhibition could have altered the subcellular distribution of PS1, thereby segregating it from proteasome-mediated degradation, although the precise localization of PS1 after PI3K inhibition was not clarified in this study. It has previously been demonstrated that PS1 is degraded by the proteasome upon binding of msel-10 and following poly-ubiquitination [16]. It is un-

clear whether msel-10 is involved in the multiple-mono-ubiquitination of PS1 under PI3K inhibition. In addition, whether GSK-3β-mediated direct phosphorylation of PS1 [14,22,23] is involved in this mode of ubiquitination needs to be clarified. The physiological significance of the ubiquitination of PS1 under PI3K inhibition can be an interesting target of future study.

References

[1] F. Acconcia, S. Sigismund, S. Polo, Ubiquitin in trafficking: the network at work, Exp. Cell Res. 315 (2009) 1610–1618.
[2] L. Baki, J. Shioi, P. Wen, Z. Shao, A. Schwarzman, M. Gama-Sosa, R. Neve, N. Robakis, PS1 activates PI3K thus inhibiting GSK-3 activity and tau overphosphorylation: effects of FAD mutations, EMBO J. 23 (2004) 2586–2596.
[3] A. Bergman, E. Hansson, S. Pursglove, M. Farmery, L. Lannfelt, U. Lendahl, J. Lundkvist, J. Näslund, Pen-2 is sequestered in the endoplasmic reticulum and subjected to ubiquitylation and proteasome-mediated degradation in the absence of presenilin, J. Biol. Chem. 279 (2004) 16744–16753.
[4] R. Bhat, S. Budd Haeberlein, J. Avila, Glycogen synthase kinase 3: a drug target for CNS therapies, J. Neurochem. 89 (2004) 1313–1317.
[5] D. Edbauer, E. Winkler, J. Regula, B. Pesold, H. Steiner, C. Haass, Reconstitution of gamma-secretase activity, Nat. Cell Biol. 5 (2003) 486–488.
[6] W. Esler, W. Kimberly, B. Ostaszewski, T. Diehl, C. Moore, J. Tsai, T. Rahmati, W. Xia, D. Selkoe, M. Wolfe, Transition-state analogue inhibitors of gamma-secretase bind directly to presenilin-1, Nat. Cell Biol. 2 (2000) 428–434.
[7] R. Francis, G. McGrath, J. Zhang, D. Ruddy, M. Sym, J. Apfeld, M. Nicoll, M. Maxwell, B. Hai, M. Ellis, A. Parks, W. Xu, J. Li, M. Gurney, R. Myers, C. Himes, R. Hiebsch, C. Ruble, J. Nye, D. Curtis, Aph-1 and pen-2 are required for Notch pathway signaling, gamma-secretase cleavage of betaAPP, and presenilin protein accumulation, Dev. Cell 3 (2002) 85–97.
[8] M. Glickman, A. Ciechanover, The ubiquitin-proteasome proteolytic pathway: destruction for the sake of construction, Physiol. Rev. 82 (2002) 373–428.
[9] C. Goutte, Genetics leads the way to the accomplices of presenilins, Dev. Cell 3 (2002) 6–7.
[10] G. He, H. Qing, F. Cai, C. Kwok, H. Xu, G. Yu, A. Bernstein, W. Song, Ubiquitin-proteasome pathway mediates degradation of APH-1, J. Neurochem. 99 (2006) 1403–1412.
[11] G. He, H. Qing, Y. Tong, F. Cai, S. Ishiura, W. Song, Degradation of nicastrin involves both proteasome and lysosome, J. Neurochem. 101 (2007) 982–992.
[12] T. Jensen, M. Loo, S. Pind, D. Williams, A. Goldberg, J. Riordan, Multiple proteolytic systems, including the proteasome, contribute to CFTR processing, Cell 83 (1995) 129–135.

[13] J. Johnston, C. Ward, R. Kopito, Aggresomes: a cellular response to misfolded proteins, J. Cell Biol. 143 (1998) 1883–1898.

[14] F. Kirschenbaum, S. Hsu, B. Cordell, J. McCarthy, Glycogen synthase kinase-3beta regulates presenilin 1 C-terminal fragment levels, J. Biol. Chem. 276 (2001) 30701–30707.

[15] R. Kohno, H. Sawada, Y. Kawamoto, K. Uemura, H. Shibasaki, S. Shimohama, BDNF is induced by wild-type alpha-synuclein but not by the two mutants, A30P or A53T, in glioma cell line, Biochem. Biophys. Res. Commun. 318 (2004) 113–118.

[16] J. Li, A. Pauley, R. Myers, R. Shuang, J. Brashler, R. Yan, A. Buhl, C. Ruble, M. Gurney, SEL-10 interacts with presenilin 1, facilitates its ubiquitination, and alters A-beta peptide production, J. Neurochem. 82 (2002) 1540–1548.

[17] Y. Li, M. Xu, M. Lai, Q. Huang, J. Castro, J. DiMuzio-Mower, T. Harrison, C. Lellis, A. Nadin, J. Neduvelil, R. Register, M. Sardana, M. Shearman, A. Smith, X. Shi, K. Yin, J. Shafer, S. Gardell, Photoactivated gamma-secretase inhibitors directed to the active site covalently label presenilin 1, Nature 405 (2000) 689–694.

[18] P. Marambaud, K. Ancolio, E. Lopez-Perez, F. Checler, Proteasome inhibitors prevent the degradation of familial Alzheimer's disease-linked presenilin 1 and potentiate A beta 42 recovery from human cells, Mol. Med. 4 (1998) 147–157.

[19] C. Pickart, Ubiquitin enters the new millennium, Mol. Cell 8 (2001) 499–504.

[20] H. Steiner, E. Winkler, D. Edbauer, S. Prokop, G. Basset, A. Yamasaki, M. Kostka, C. Haass, PEN-2 is an integral component of the gamma-secretase complex required for coordinated expression of presenilin and nicastrin, J. Biol. Chem. 277 (2002) 39062–39065.

[21] N. Takasugi, T. Tomita, I. Hayashi, M. Tsuruoka, M. Niimura, Y. Takahashi, G. Thinakaran, T. Iwatsubo, The role of presenilin cofactors in the gamma-secretase complex, Nature 422 (2003) 438–441.

[22] C. Twomey, J. McCarthy, Presenilin-1 is an unprimed glycogen synthase kinase-3beta substrate, FEBS Lett. 580 (2006) 4015–4020.

[23] K. Uemura, A. Kuzuya, Y. Shimozono, N. Aoyagi, K. Ando, S. Shimohama, A. Kinoshita, GSK3beta activity modifies the localization and function of presenilin 1, J. Biol. Chem. 282 (2007) 15823–15832.

[24] C. Ward, S. Omura, R. Kopito, Degradation of CFTR by the ubiquitin-proteasome pathway, Cell 83 (1995) 121–127.

[25] C. Weihl, G. Ghadge, S. Kennedy, N. Hay, R. Miller, R. Roos, Mutant presenilin-1 induces apoptosis and downregulates Akt/PKB, J. Neurosci. 19 (1999) 5360–5369.

[26] M. Wolfe, W. Xia, B. Ostaszewski, T. Diehl, W. Kimberly, D. Selkoe, Two transmembrane aspartates in presenilin-1 required for presenilin endoproteolysis and gamma-secretase activity, Nature 398 (1999) 513–517.